Analysis of non-equilibrium foamy oil behavior in pressure depletion processes

by

Tong Chen

A thesis submitted in partial fulfillment of the requirements for the degree of

Master of Science

in

Petroleum Engineering

Department of Civil and Environmental Engineering
University of Alberta

Abstract

Cold Heavy Oil Production with Sand (CHOPS) is considered to be a promising non-thermal primary-recovery technique, in western Canada and Venezuela. However, it offers low oil recovery factor (only 5 to 15%) and creates high porosity and high permeability channels known as wormholes. Further approaches are entailed (post-CHOPS) to increase oil recovery. Thermal methods and waterflooding are not efficient and economical due to heterogeneity and reservoir instability. Cyclic Solvent Injection (CSI) is the most commonly used method for post-CHOPS process. Non-equilibrium foamy oil behavior (i.e., solvent dissolution/exsolution) and solvent transport are two dominant recovery mechanisms for CSI processes in post-CHOPS reservoirs. The trapped gas bubbles generated during the pressure depletion stage are the typical characteristics of foamy oil flow. Although a number of models were developed in the past to describe the dissolution of solvent and bubble formation, calibration of these models against actual observations remain challenging. Many existing solvent technologies suffer from low production rates due to limited solvent /heavy oil interaction. Improving our understanding of solvent dissolution/exsolution under different pressure conditions would aid in the design of operating strategies (e.g., pressure depletion and solvent injection schemes) for enhanced solvent/oil mixing and transport.

A detailed mechanistic simulation model is constructed and calibrated against a set of experimental measurements. The fluid model is defined based on equilibrium saturation pressures and gas-oil ratios corresponding to different combinations of solvent and dead oil. The viscosity model is formulated using measurements at different temperatures and solvent-oil mixtures. Reaction kinetics is implemented to represent the non-equilibrium exsolution of gas from solution gas to

bubble gas and free gas in foamy oil flow. The simulation model predicts a delay in free gas formation in the sand pack, as observed in the experimental program. Propane-based and carbon dioxide-based solvent mixtures exhibit significant foamy oil characteristics, enabling the oil viscosity to remain close to its live oil value. The rates of gas exsolution and oil production are strongly dependent on the pressure depletion schedule, as well as the solvent compositions and properties.

Next, a field scale post-CHOPS model is constructed and upscaled from the core model to analyze the impacts of simulation scales, heterogeneous wormholes, and the operating schedules on foamy oil behavior of different solvent systems. A fractal wormhole network is modeled. To analyze the impacts of pressure depletion strategies, single stage pressure depletion involving three live oil-solvent systems, as well as two cycles of CSI production processes, are examined. Detailed sensitivity analyses involving different solvent compositions are discussed. Similar as the observations from core model: the results illustrate that both C_3H_8-based and CO_2-based solvents performe significant non-equilibrium foamy oil behaviors; the amount of foamy oil flow is strongly dependent on the pressure depletion rate. On the contrary to the core models, where CO_2 outperforms C_3H_8 (as no C_3H_8 bubbles could be observed), the field-scale simulations show comparable recovery performance for both C_3H_8-based and CO_2-based solvents. The developed simulation is useful for providing important insights regarding the interplay between wormhole heterogeneity, time scale and non-equilibrium solvent dis(ex)solution on the characteristics of foamy oil flow and oil recovery at the field level.

Dedication

In dedication to my dearest parents: Yongsheng Chen and Aihong Li, who always encourage me to pursue my dreams and empower me never give up when encountering challenges in life. Without their endless love, inspiration, understanding and great support, these wonderful and memorable experience would not happen.

Acknowledgements

First and foremost, I would like to express my profound gratitude, appreciation and a message of thanks to my Supervisor, Dr. Juliana Y. Leung. She has been the greatest supporter and leader of this research. I am so appreciated for my Supervisor providing me a precious opportunity to study in her research group. I am really beneficial from her patient guidance and bright research ideas. I am also grateful for her continuous support, encouragement and understanding throughout my research study.

I would like to thank Dr. Japan Trivedi and Dr. Alireza Nouri for being part of my examination committee. Their constructive suggestions and comments are always appreciated.

I am also thankful to all my colleagues and friends for their suggestions, assistance and encouragement. I have experienced a really wonderful and memorable time with them.

In addition, I would also like to thank University of Alberta Future Energy Systems (FES) for financially supporting the project and Computer Modeling Group (CMG) for providing the academic licenses for STARS and WinProp.

Table of contents

List of Tables

List of Figures

Nomenclature

Symbols

T_b	=	Normal Boiling Point (°C)
T_c	=	Critical Temperature (K)
P_c	=	Critical Pressure (atm)
ω	=	Acentric Factor
M	=	Molecular Weight (g/mole)
m	=	Mass Weight (g)
ρ	=	Density (g/cm^3)
n	=	Mole Numbers
P_b	=	Bubble Point Pressure (kPa)
P_b'	=	Pseudo-Bubble Point Pressure (kPa)
r_k	=	Kinetic Reaction Constant
E_{ak}	=	Activation Energy
$\prod$	=	Production Operator
S_{gc}	=	Critical Gas Saturation
R	=	Universal Gas Constant
N	=	Order of Component
C	=	Molar Concentration of Component

Subscripts

G/g	=	Gas Phase
L/o	=	Oil Phase
w	=	Water
i/j	=	Index of Solvent Component
n	=	Total number of Solvent Components
x,y,z	=	Coordinates

Acronyms

CHOPS	=	Cold Heavy Oil Production with Sand
EOR	=	Enhanced Oil Recovery
OOIP	=	Original Oil in Place
MW	=	Molecular Weight
SG	=	Specific Gravity
CSI	=	Cyclic Solvent Injection
JST	=	Jossi Stiel Thodos
PVT	=	Pressure Volume Temperature
UCSS	=	Unconsolidated Sandstone
NMR	=	Nuclear Magnetic Resonance
PCPs	=	Progressing Cavity Pumps
GOR	=	Gas Oil Ratio
DLA	=	Diffusion-Limited Aggregation

PAW	=	Probabilistic Active Walker
DWM	=	Dynamic Wormhole Module
CSS	=	Cyclic Steam Stimulation
SAGD	=	Steam-Assisted Gravity Drainage
VAPEX	=	Vapor Extraction
GA-CSI	=	Gas Flooding-Assisted Cyclic Solvent Injection
AITF	=	Alberta Innovates-Technology Futures
FD	=	Fast Depletion
SD	=	Slow Depletion

Chapter 1. Introduction

1.1 Background and Motivation

Cold heavy oil production with sand (CHOPS) is a non-thermal primary production approach to produce heavy oil from thin and unconsolidated reservoirs in Western Canada and Venezuela. This method successfully initiates continuous sand production along with oil under the huge draw down pressure caused by the progressive cavity pump. CHOPS approach is a proven primary heavy oil production technology. It has manifested great economic advantages with an average ultimate oil recovery of 5% to 10% (Istchenko and Gates, 2012), which means that approximately 90% of the original oil in place is still left in the reservoir. Therefore, further follow-up EOR techniques are required to recover the additional heavy oil in reservoir.

Production of large amount of sands during CHOPS leaves the wormhole network structures (Smith, 1988; Dusseault, 1993; Lebel, 1994; Yeung, 1995). The generated high permeability and high porosity channels are not suitable for applying waterflooding and thermal-based EOR methods. Several technical problems are associated with these methods, for instance, extensive heat loss, large energy and water consumption and uneconomic water treatment. Cyclic solvent injection has been widely accepted as the best post-CHOPS EOR methods in terms of the oil production, energy efficiency, produced oil quality and environmental benefits comparing with other follow-up methods (Haskin et al., 1989; Yu et al., 2016; Chang et al., 2013; Du et al., 2018). The mechanisms of post-CHOPS are known as foamy oil flow, viscosity reduction, solution gas drive, gravity force drive, swelling effect as well as diffusion and dispersion effect (Jia et al., 2013;

Hong et al., 2017). Foamy oil is not only encountered during primary CHOPS production through evolving methane originally in oil but also applied in the post-CHOPS CSI processes and it is an important mechanism for heavy oil production. Many work has been done to study the influence of pressure decline rate, solvent type, injection rate, injection time and soaking time on CSI performance. The non-equilibrium process is effected by the kinetics of bubble nucleation and gas diffusivity. This non-equilibrium behavior is likely to be more important in laboratory experiments, because lab-scale, which are run on a smaller time scale compared with field case (Maini, 2001).

Laboratory pressure depletion tests in sand pack are operated to study the non-equilibrium solvent behavior. Although several experimental and numerical work were conducted on pressure depletion processes, there are inconsistence regarding the potential of oil production for different types of solvents and the effects depletion rate on foamy oil formation and oil production. The kinetic models are preferred due to the ability of capturing the non-equilibrium and time-dependent characteristics associated with foamy oil flow. Due to lack of detailed laboratory data to clarify the physics of the process and support numerical simulation studies, the effects of different solvents on heavy oil production under different pressure depletion conditions require further analysis.

Many existing solvent technologies suffer from low production rates due to limited solvent /heavy oil interaction. Improving our understanding of solvent dissolution/exsolution under different pressure conditions would aid in the design of operating strategies (e.g., pressure depletion and solvent injection schemes) for enhanced solvent/oil mixing and transport.

1.2 Problem Description

Foamy oil is not only encountered during primary CHOPS production through evolving methane originally in oil but also applied in post-CHOPS processes by cyclically injecting different types of solvents. Despite the remarkable investigations on foamy oil, the mechanisms of foamy oil flow in sand pack are not understood clearly yet. Besides, as there is lack of detailed and valid data of core scale experiments to support the numerical studies on foamy oil behavior, calibration of these models against actual experimental data are needed.

Except for the simulation study on the non-equilibrium foamy oil behavior in sand pack, modeling of solvent dissolution and exsolution under different pressure conditions at the field level should also be considered. Better understanding the non-equilibrium foamy oil behavior in field-scale reservoir would be beneficial for designing the operating strategies (e.g., pressure depletion and solvent injection schemes) for enhanced solvent/oil mixing and transport.

1.3 Research Objectives

First step of this research is to construct a detailed mechanistic simulation model and calibrated against experimental measurements from a set of pressure depletion tests conducted in both bulk fluid systems and porous media. Reaction kinetics in STARS model were implemented to represent the non-equilibrium solvents (CH_4, C_3H_8 and CO_2) dissolution and exsolution from solution gas to dispersed gas bubbles and free gas in foamy oil flow. Different combination of solvent mixtures and pressure depletion rates are examined in the sand pack model. Next, a scaled-up simulation study is conducted in a typical post-CHOPS field-scale reservoir. To analyze the

impacts of simulation scales, heterogeneous wormholes, and the operating schedules on foamy oil behavior of different solvent systems. Single stage pressure depletion involving three live oil-solvent systems, as well as two cycles of CSI production processes, are examined. The specific objectives have been addressed below:

(1) Construct fluid models of three live oil-solvent systems based on a series of experimental measured pressure/volume/temperature (PVT) and viscosity data. These tuned fluid models are used to construct numerical simulations of sand pack and field depletion processes.

(2) Construct a detailed mechanistic simulation model and calibrated against experimental measurements from a set of pressure depletion tests conducted in both bulk fluid systems and porous media. Tune the kinetic reaction constants to history match the oil viscosity profile, pressure depletion schemes, oil rate and oil production profile.

(3) Conduct pressure depletion tests for Solvent 1 and Solvent 2 systems as well under both fast and slow depletion schemes. Then, compare foamy oil behaviors corresponding to the three live oil-solvent systems in terms of oil viscosity, bubble gas mole fraction and oil recovery factor.

(4) Analyze the effects of solvent compositions and operating schedules on recovery efficiency.

(5) Construct a field scale model according to a typical post-CHOPS reservoir model with wormholes distributed in the middle layer of the reservoir to analyze the impacts of simulation scales, heterogeneous wormholes, and the operating schedules on foamy oil behavior of different solvent systems.

(6) Perform single stage pressure depletion tests as well as two cycles of post-CHOPS CSI processes to observe the foamy oil behavior involving of the three solvent systems in field scale reservoir.

1.4 Thesis outline

Chapter 1 covers the background and motivation of this research, introducing the problem description, explaining the research objectives that should be achieved ultimately.

Chapter 2 presents a comprehensive literature review of Cold Heavy Oil Production with Sand (CHOPS), including the previous studies on CHOPS, the dynamic wormhole growth and the modeling approaches of CHOPS; then describes the foamy oil flow as well as the post-CHOPS CSI processes in terms of experimental and numerical study.

Chapter 3 describes the referred laboratory experiments, including the description of the specific experimental procedures: dead oil and live oil preparation, foamy oil viscosity measurement using NMR and pressure depletion tests in bulk fluid systems and in porous medium; then detailed experimental data in terms of fluid properties and sand pack properties were summarized.

Chapter 4 describes the main simulation work of this research, including fluid model generation and the explanations of feed mole fraction number calculation and fluid model matching results; illustrate the construction of sand pack model and analysis the history matching results and the effects of solvent compositions on oil recovery.

Chapter 5 illustrates pressure depletion tests in field level and analyzes the differences of foamy oil behavior for three live oil-solvent systems between sand pack and field models. Two cycles of CSI tests observe the impacts of the bubble gas component in dynamic processes on oil recovery.

Chapter 6 finally presents the conclusions and main contributions of this work and the recommendations for future work.

1.5 Novelties and Contributions

This work presents a detailed mechanistic simulation model which is calibrated against experimental measurements from a set of pressure depletion tests conducted using both bulk fluid systems and porous media. Although a number of kinetics models are available to describe the dissolution and exsolution of solvent and bubble formation, calibration of these models against actual observations remain challenging. Besides, the analysis of depletion tests in field scale model is not sufficient, this scaled-up study on the characteristics of the non-equilibrium foamy oil behavior provide better understanding of the solvent dissolution and exsolution under different pressure conditions at the field level. The observations from both sand pack and field scale models would be beneficial for designing the operating strategies (e.g., pressure depletion and solvent injection schemes) for enhanced solvent/oil mixing and transport.

Chapter 2. Literature Review

2.1 Cold Heavy Oil Production with Sand (CHOPS)

Cold Heavy Oil Production with Sand (CHOPS) is a non-thermal primary production technique widely used for heavy oil recovery in western Canada and Venezuela, where the oil viscosity ranges from 1000 mPa·s to about 50,000 mPa·s (Haddad et al., 2015). Field production has demonstrated that aggressive sand production improves the recovery performance. The development and adoption of progressing cavity pumps (PCPs) that enables CHOPS higher productivity. Before utilizing PCPs, operators used the beam pumping then some sand-excusive devices, such as: gravel packs, screens and slotted liners, because at that time, it was believed that the sand production should be avoided (Geilikman et al., 1994). But after the wells were produced under CHOPS using PCPs, oil production rates had been increased up to 10 times seen in the Celtic field operated by Mobil Canada. The results of field production suggest that there is a linear relationship between sand-production rate and oil production, therefore, operators have often attempted to maximize the sand-production rate while maintaining wellbore stability to maximize the oil recovery (Loughead and Saltuklaroglu., 1992).

2.1.1 Experimental and Field Studies on CHOPS

Two main mechanisms contribute to the high primary production: one is the formation of high permeability channel-like structures, known as “wormholes”; the other mechanism is due to the delayed gas exsolution, known as “foamy oil” drive (Sarma and Maini, 1992; 1993; Tremblay et al., 1996). The formation of wormholes has been shown to exist in laboratory experiments as well

as the field pilot tests conducted with fluorescein dyes. Researchers had postulated that the improved oil production can be explained by an enhanced-permeability zone in the near-wellbore region resulted from sand production. The enhanced-permeability zone can take the form of a disturbed zone around the wellbore with one or more high-permeability channels (Dusseault and El-Sayed, 1999). Foamy oil flow aids in mobilizing sand and reservoir fluids, leading to the formation of wormholes. The solution gas oil ratio is relatively high, typically between 10 and 20 m^3/m^3, which provides the ability for the onset of foamy oil flow in turn lower effective oil viscosity. Numerous field and laboratory studies were conducted to investigate the mechanisms of CHOPS process.

Laboratory experiments reveal that in the unconsolidated sand packs, high-permeability channels can form under appropriate conditions. Tremblay (1998) conducted experiments illustrating the evolution of wormholes in sand packs, which grow dominantly within areas of higher porosity. Porosity and unconfined compressive strength are inversely rated, indicating the wormholes grew within the areas of lowest compressive strength (Tremblay, 1997). These experiments did aid in conceptualizing the wormholes, which were postulated to occur on the basis of laboratory and field studies, and also assisted in understanding the mechanisms of CHOPS. Field tracer tests demonstrated high connectivity of the neighboring wells with effective permeabilities only achievable by open channels within the reservoir. Tracer tests analyses in CHOPS wells during drilling close to the wells had been operated earlier by sand production, and the analysis of drilling conditions such as cement flow rate, confirmed the existence of the open channels (Squires, 1993; McCaffery and Bowman, 1991; Metwally and Solanki, 1995). Tremblay (1996; 1997; 1998; 1999) and Mazurek (1994) found that wormholes are created during oil production and the growth rate is proportional to the oil rate. They also concluded that most of the oil flow happens at the tip of

reservoir where the growth is fastest and the diameter of the wormholes are main constant throughout the entire production process. Therefore, they realized that the average sand flux at the tip of wormholes is proportional to the pressure gradient at the tip. Consequently, once the pressure gradient reaches its critical minimum surface erosional gradient or if the pressure gradient inside is not sufficient to transport sands to production well, the wormhole growth stops.

A typical production profile of the typical CHOPS well in the Western Canadian Heavy oil belt is displayed in Figure 2.1 (Istchenko et al., 2014), which reveals that the oil production rate reaches the peak value as sand production increases and with sand production, wormholes are generated within the reservoir result in a high pressure drop along the length of the wormholes. The water rate increases after several years after it overshadows the oil rate, which is the signal of the end of economic life of the process (Haddad et al., 2015).

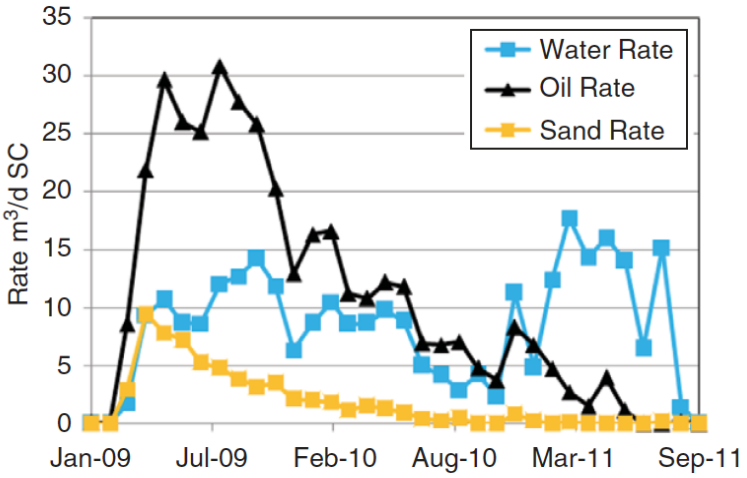

Figure 2. 1 An example of a typical production profile for a CHOPS well in eastern Alberta, Canada. (Istchenko et al., 2014)

2.1.2 Dynamic Wormhole Growth

The process of Cold Heavy Oil Production with Sand generates sharp pressure gradients, following with the sand matrix failures in areas of relative weak cohesion strengths, and the inflow of high viscous fluid dragged the failed sand to the wellbore. Therefore, this will lead to aggressive sand productions along with heavy oil in the initial stage of heavy oil production (David, 2018). The high permeability channels generated during the sand and oil production from the unconsolidated reservoirs are known as "wormholes" (Sawatzky et al., 2002). The wormhole extension and growth into the reservoir with different ranching network are dependent on the pressure distribution outside the wormholes and the inherent reservoir heterogeneity (Yuan et al, 1999; Rangriz and Babadagli, 2014). Presence of a wormhole network among wells were investigated in earlier studies based on field observations. To effectively characterize the wormhole growth in cold production, Tremblay et al. (1999) visualized the formation and growth of a wormhole under solution gas drive using a CT scanner in laboratory. The CT images and production results revealed that gas evolution into bubbles during pressure depletion tests reduced the pressure gradient and eventually destabilized sand grains at the wormhole tip. Several studies (Kantzas and Brook, 2004; Tremblay 2007; Rangriz and Babadagli, 2014) showed that wormholes likely growth from well perforations as a consequence of sand production and extend to the weakest sand formation. In conclusion, the wormholes grow in regions of the weakest matrix and towards the highest-pressure gradient in the formation. Moreover, Sawatzky et al. (2002) discussed two possible stages of wormhole network development. The first stage corresponds to a period when the pressure difference is substantially large enough for the fast growth of the wormholes. The type of flow in this stage is more like the lug flow. While in the second stage, the flow of oil and lose sand can be approximated as stratified flow. During this period, the increasing wormhole numbers with

constant bottom-hole pressure makes the pressure the channel tip too small. Finally, the small pressure gradient stops the further wormhole growth.

2.1.3 Modeling of Cold Heavy Oil Production

Recent years several CHOPS models were developed and validated. Vardoulakis et al. (1996) presented a mathematical model on the basis of mass balance of produced sands, flowing fluid, basic particles erosion laws and Darcy's Law in porous medium. Tremblay and Olakowski (2003) built a wormhole growth model composed of a fluid drainage equation and a sand fluidization equation. Other models, such as hydro-geomechanics (Coombe et al., 2001) and reservoir-geomechanics (Wang and Xue., 2002) have provided formative results that assist with the understanding of cold production. However, these models could not predict the wormhole growth and patterns in an unconsolidated formation. The probabilistic active walker (PAW) model could describe the wormhole development pattern, which brought new aspect to understanding wormhole growth and cold production of heavy oil (Yuan et al., 1999). Liu and Zhao (2005) proposed the diffusion-limited aggregation (DLA) model which developed the physics of a wide variety of branching-growth patterns. Tremblay (2005) used predefined geometries to model sand transport through wormholes. One key limitation of these models was that the wormhole geometry is predefined, which cannot be controlled by the physics of wormhole growth. A dynamic wormhole module (DWM) was created which allows for the wormholes to be grown dynamically as an extending production well. The module is automated and retrieved all the relevant data for a complete restart of the simulation as well as any information needed to determine growth criterion

(Istchenko and Gates., 2012). These models have provided informative results which assisted to better understand the mechanisms of CHOPS in unconsolidated reservoirs.

2.2 Foamy Oil Flow

Foamy oil flow is a non-Darcy form of two-phase flow encountered in Canadian and Venezuelan-heavy oil reservoirs. The mechanisms are similar to solution gas drive in conventional reservoirs. The term "foamy oil" originated from observations of foams in samples collected at the wellhead (Sara and Maini, 1992). It was coined to distinguish the two-phase oil/gas flow in a porous media of such heavy oils from the normal two-phase behavior (Maini, 2001). Smith (1988) appears to be the first to publish a detailed analysis of such unusual production behavior. He attributed it to the flow characteristics of heavy oil containing a large volume fraction of tiny gas bubbles. He also suggested that the dispersed small bubbles in heavy oil could be several-fold higher than the single-phase oil mobility. Maini et al. (1993) attempted to verify the assertion of high dispersion mobility in the laboratory but found that the presence of freshly nucleated gas bubbles decreased the oil mobility, a composite result was observed. However, they found that the dispersed gas bubbles were indeed possible under solution gas drive conditions. Therefore, the flow behavior of such unusual behavior has become a subject of several investigations and considerable speculation (Metwally and Solanki, 1995; Huerta et al., 1996; Urgelli et al., 1999; Alvartamani et al., 1999; Sheng et al., 1999; Du and Yortsos, 1999; Bora et al., 2003), but at that time the foamy oil mechanisms remained poorly understood and controversial. There are two types of non-equilibrium processes involved in the foamy oil solution gas drive in heavy oils (Maini, 2001). The non-equilibrium between solution gas and free gas leads to a possibility of significant supersaturation of the dissolved gas in the oil phase. The non-equilibrium process is effected by the kinetics of bubble nucleation and gas diffusivity. This non-equilibrium behavior is likely to be

more important in laboratory experiments, because lab-scale, which are run on a smaller time scale compared with field case. The other mechanism is related to fluid distribution in the rock (Maini, 2001). Because of high oil viscosity and high drawdown pressure in the cold production, the local capillary number can be high enough to mobilize the isolated gas bubbles, which leads to the dispersed flow. This non-equilibrium process is affected by the surface tension of the oil, the absolute permeability and the gradient value of the flow in the vicinity of the isolated bubbles. Both of the above two non-equilibrium processes are essential for foamy oil solution gas drive. The non-equilibrium related to the bubble nucleation and growth becomes less significant when the time scale moves from a few hours or a few days to in the laboratory scale to years in field. However, the other non-equilibrium process s not directly affected by the time scale, so it is equally important in both laboratory and in the field, provided similar rock/fluid properties and pressure gradients are involved (Maini, 2001). The second non-equilibrium process was considered to be more important in causing the anomalous production behavior in the field.

2.2.1 Experimental Study and Field Observations

During the past several decades, foamy oil drive has been studied intensively by investigating two kinds of non-equilibrium presentation forms according to Maini (2001), they are supersaturation and fluid distribution in porous media, respectively. Previous experimental tests in the laboratory mainly focused on the heavy oil-methane system (Liu et al., 2013; Ostos et al., 2005; Xu, 2007; Tang et al., 2005), which was studying the performance of heavy oil cold production. The gas rate is an important parameter to differentiate the characteristics of foamy oil and conventional solution gas drive. Maini (1999) operated an experiment in order to better understand the difference between the conventional solution gas drive and the foamy oil drive. He observed that when the pressure declined to the pseudo-bubble point pressure, a bubble nucleation process occurs in the

pore and only a few grow out of the cavities for the foamy oil flow. A number of factors which would affect the foamy oil behavior were studied, which included the pressure depletion rates, solvent types and compositions, critical gas saturation, compressibility, etc. The non-equilibrium phenomenon of the methane-based foamy oil phase behavior in bulk fluid system measurement and fluid flow behavior in physical porous medium simulation have been characterized. The experimental characterizations have been quite mature to predict the methane-based live oil pressure depletion tests in laboratory measurements. Wong et al. (1999) has proposed the method to calculate the total compressibility in a heavy oil reservoir. Bennion et al. (2003) conducted PVT measurement on methane-based live oil under different pressure decline rates. Sheng (1997) measured the methane-based foamy oil properties form different perspectives in terms of foamy oil stability, foamy oil compressibility, initial GOR effect, pressure depletion rate effect and so on. These experimental tests all found that for methane based live oil system, the higher pressure decline rate applied, the longer the endurance of foamy oil flow as well as higher stability, compressibility and GOR during the existence of foamy oil flow. In terms of porous media tests, Busahmin and Maini (2010) and Sun et al. (2013) have tested their live oil samples at the same pressure decline rates in accordance with PVT measurements. Ostos (2003) and Xu (2007) examined the effect of capillary number and the presentation in the long sand pack pressure depletion tests. Compared with methane-based live oil systems, propane-based solvent has been observed that it has a higher solubility into heavy oil. Unlike methane-based solvent component which were extensively investigated in laboratory and field pilot tests, propane-based solvent is usually used as a very crucial solvent component in CSI process (Wang et al., 2015). Zhou et al. (2016) investigated the impact of pressure depletion rates on different heavy oil-solvent systems in porous media, the schematic of the foamy oil flow experimental setup is shown in Figure 2.2.

They have observed that the foamy oil behavior of the heavy oil-mixture system is poorer than heavy oil-methane and heavy oil-propane system.

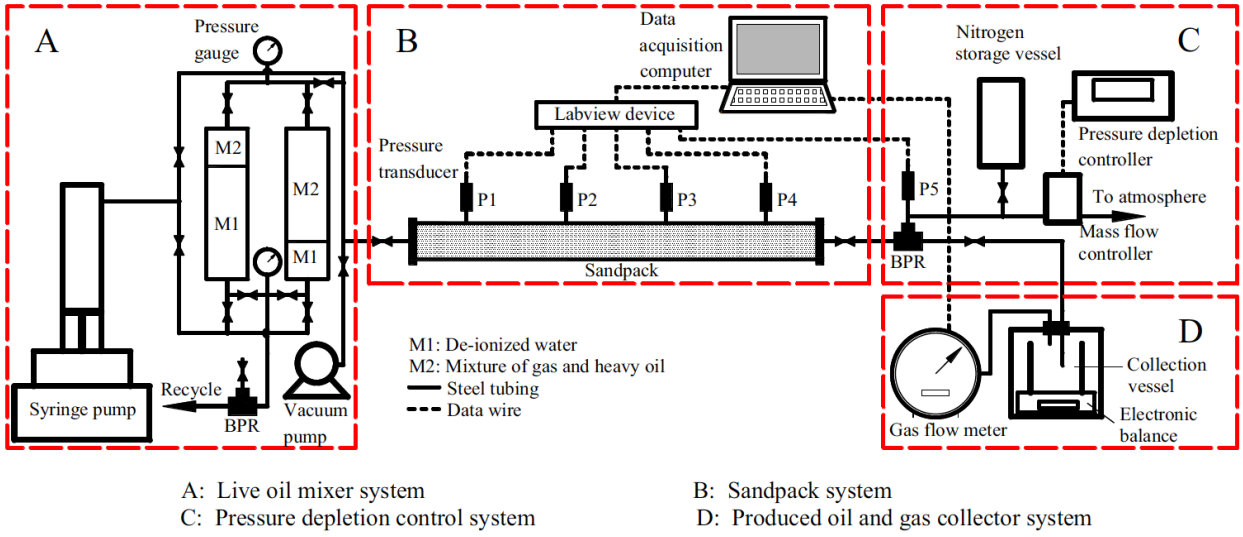

Figure 2. 2: Schematic of the foamy oil flow experimental setup (Zhou et al., 2016)

For the field case study, the most notable field observation is that some unconsolidated-sand heavy oil reservoirs, exploited with vertical wells under primary depletion conditions, performs better when sand is allowed to flow freely into the wells (Maini, 2001). Oil production rates have been reported to be more than 10 times the flow rate predicted by Darcy's law. The sand production can increase fluid mobility in the near wellbore area by increasing the permeability in the attached zone. During the cold production, the oil/water/sand/gas mixture is produced as foamy mass, which goes to a stock tank for gravity segregation. Past field study also observed that similar reservoirs that were produced earlier with sand control yielded much lower recovery factors. Without sand production, the reservoir pressure declined more rapidly. With sand production, the GOR increases slowly throughout the depletion process (Maini, 2001).

2.2.2 Numerical Simulation of Foamy Oil Flow

Over the past several years, numerous efforts have been made to understand and model the mechanism of solution gas drive in primary heavy oil recovery (Maini et al., 2001). Two phase flow of oil and gas mixtures is described by relative permeability relationships, with the adjustments of relative permeability curves and rock fluid properties such as critical gas saturation, rock and fluid compressibility, pressure dependent oil viscosity, absolute permeability and bubble point pressure (Loughead and Saltuklaroglu, 1992).

2.2.2.1 Pseudo Bubble Point Models

Kraus et al. (1993) generated a pseudo bubble point model for the primary depletion process in foamy oil reservoir. The model should satisfy some requirements that all the released solution gas remains entrained in the oil phase until the reservoir pressure drops to the pseudo-bubble point pressure; below the pseudo-bubble point pressure, only a small fraction of released gas is trapped in heavy oil; and the gas fraction decreases linearly to zero with declining pressures. The entrained gas is treated as a part of the oleic phase. This type of foamy oil model considers the gas molar volume and compressibility of the dispersed gas bubbles, and uses the diffusion equations to calculate the reservoir depletion performance. The equilibrium ratios from the conventional pressure/volume /temperature (PVT) data are modified according to the pseudo-bubble point pressure (Maini, 2001). From the results of a primary depletion in a volumetric reservoir using foamy oil properties in a reservoir simulator, three anomalous production characteristics observed for foamy oil reservoirs namely high oil recovery, low producing GOR and natural pressure maintenance. However, this kind of model fails to the dynamic processes of bubble nucleation, bubble growth and bubble coalescence.

2.2.2.2 Modified Fractional Flow Models

The fractional flow curve and the gas/oil relative permeability curves are modified to match the foamy oil production behavior. Lebel (1994) created a model which assumed that all the released gas remains trapped in oil up to a certain system-dependent limiting volume fraction. The gas saturation increases from zero and the fractional flow of gas increases linearly with saturation until the limitation entrained gas saturation is reached. When the gas saturation increases over the limited saturation, the free gas will come out. The effective oil viscosity was assumed to decrease marginally as gas volume fraction increases. The equilibrium PVT properties are applicable in this model, and this model is equivalent to the gas relative permeability curve up to a certain adjustable gas saturation. Firoozabadi (2001) and Pooladi-Darvish (1999) advocated a similar model based on relative permeability approach. They assumed that the relative permeability concept can be applied to the dispersed gas flow. However, the predetermined gas oil relative permeability curve cannot describe the field condition in which the capillary number varies with time and position in the reservoir.

2.2.2.3 Reduced Viscosity Models

Claridge and Prats (1995) attempted to the abnormal higher inflow rates, and they discussed that the asphaltenes present in the curde oil adhere to the gas bubbles while the latter are still very tiny. The coating of asphaltenes on the bubble surfaces stabilize the bubbles at a small size. They have explained that the oil viscosity decreases dramatically because of the removal of the dispersed asphaltenes. This micro physics were just under assumption and not proved by experiments. Moreover, Shen and Batcycky (1996) formulated the theory of lubrication in an attempt to show that the apparent viscosity decreasing of oil and gas mixture at a low gas fraction is due to the

lubrication effect of gases coming out of solution. And this gas lubrication requires the existence of microbubbles attached to the wall of pores, which has not been approved through experiment evidence.

2.2.2.4 Kinetic Models

The dispersion of gas in oil is not a thermodynamic stable species and by given enough time with helpful environment, the dispersion would separate into free gas and oil phase (Maini, 2001). Kinetic models attempt to capture the time-dependent changes in the flow behavior of foamy oil. Coombe and Maini (1994) defined a three components kinetic model to account for the kinetics of physical changes occurring in the morphology of the dispersion. Three components are all in oil phase, they are dead oil, dissolved gas and dispersed gas in the form of microbubbles. The dissolved gas changes to the dispersed gas by a rate process which is drive by the local supersaturation. The second rate process is the dispersed gas changes to free gas. The STARS module in Computing Modeling Group simulator (CMG) was implemented by use of the chemical reaction routines. These two reaction processes were simulated as chemical reactions with specified stoichiometry and reaction rate constants. The rate constants should be determined through history matching. However, as this model failed to capture the time and position-dependent capillary number, it was not useful for predicting the effect of operating conditions. Sheng et al. (1999) used similar approach to model the rate of release of solution gas by exponential decay of the local supersaturation. This model was successfully history matched with laboratory solution gas drive experiments. But the the rate constants inferred by history matching are not validated for predicting the outcome of a new scenario involving different flow conditions. Joseph et al (2001) treated the dispersion gas as a pseudo single phase fluid, and Arora and Kovscek (2001) used a bubble population balance framework. Egermann and Vizika (2000) have reported some

field cased observations in the near-wellbore and in the far field regions. A model based on the capillary number dependent relative permeability cannot capture the changes in the dispersion phases, however, it might be a reasonable approximation for fully developed flow in the field.

2.3 post-CHOPS

CHOPS reservoirs offer very low oil recovery factors and a huge amount of oil (90% OOIP) is left behind in reservoir, therefore, the follow up EOR approaches are needed, known as post-CHOPS processes. Production of large amount of sands during CHOPS leaves the wormhole network structures (Smith, 1988; Dusseault, 1993; Lebel, 1994; Yeung, 1995). The generated high permeability and high porosity channels are not suitable for applying waterflooding and thermal-based EOR methods. Thermal-based heavy oil recovery methods, such as cyclic steam stimulation (CSS), steam-assisted gravity drainage (SAGD) and steam flooding etc., have been applied for more than three decades (Du et al., 2018). However, several technical problems associated with these thermal methods, for instance, extensive heat loss, large energy and water consumption and uneconomic water treatment. Thus thermal-based methods are not suitable for many heavy oil reservoirs with thin pay zones, bottom water, gas cap and low rock thermal conductivities (Lin et al., 2014). Waterflooding methods are always applied in conventional reservoir, however, the oil recovery factor for heavy oil reservoir using waterflooding method is usually low because of the displacement instability. The injected water can extremely bypass the viscous heavy oil and form water channels known as “viscous fingering”.

Solvent-based heavy oil recovery methods have some distinct advantages over the thermal-based methods in terms of the energy efficiency, produced oil quality and environmental benefits (James et al., 2007). The energy consumption is reduced by 97% in a solvent based heavy oil recovery

process in comparison with steam assisted methods (Singhal et al., 1996). Solvent-based heavy oil recovery methods are mainly classified into cyclic solvent injection (CSI), vapour extraction (VAPEX) with its variations and hybrid steam-solvent processes. VAPEX process is a solvent analogue of SAGD by dissolving a gaseous solvent into heavy oil (Butler et al., 1991). The vital shortcoming of VAPEX is the very low production rate due to low mass transfer rate and only driven by gravity force (Jiang et al., 2013). Compared with VAPEX, cyclic solvent injection (CSI), also known as haff-n-puff, has been demonstrated as the most promising and effective approach for post-CHOPS.

2.3.1 Cyclic Solvent Injection (CSI)

CSI has the highest oil production rate comparing with other EOR methods resulting from the driving mechanisms (Haskin et al., 1989; Yu et al., 2016; Chang et al.,2013; Du et al.,2018). These mechanisms are known as foamy oil flow, viscosity reduction, solution gas drive, gravity force drive, swelling effect as well as diffusion and dispersion effect (Jia et al., 2013; Hong et al., 2017). Many work has been done to study the influence of pressure decline rate, solvent type, injection rate, injection time and soaking time on CSI performance. Qazvini F and Torabi (2012) investigated the effects of the injection pressure and soaking time by fourteen huff and puff tests, what they have found were that a longer soaking time cannot increase the oil recovery noticeably with low injection pressure. Feasibility of CO_2 cyclic injection for enhancing oil recovery was examined in 1980s. Gondiken (1987) reported a pilot project with heavy oil 11 to 12 API in turkey, and the results showed that the oil production was increased by 2.5 times for two months. Lim et al., (1995); Shi et al., (2008); and Yadali Jamaloei et al., (2012) performed CSI tests by using methane, ethane, propane and corbon dioxide compare the effectiveness of the solvents. They found that ethane was effective for deasphalting and producing bitumen. Ivory et al., (2010)

injected a solvent mixture with 28 vol% C_3H_8 and 72% CO_2 in a stepped cone laboratory model (3m long), and the inside diameter of the bottom cylinder was 9.7 cm. Their results emphasized the importance of the wormholes and foamy oil flow in CSI process. Foamy oil are generated during the depressurization of heavy oil that contain dissolved gases. This mechanism and behavior of foamy oil are crucial in both primary cold production process and the post-CHOPS processes. Radial drainage tests have been conducted for CSI with oil saturated with various solvents. The tests investigated that there were similarities between the primary production of live oil and the production after injecting solvents (Bjorndalen et al., 2012). CSI is a process similar to the Cyclic Steam Simulation (CSS), which involves injecting a solvent into a single well and then a soaking period where the solvents disperse and diffuses into the oil and then producing the oil from the same well. Due to the high pressure, renewed drive energy, and the reduction in oil viscosity, the oil recovery factor is increased. Since CSI is a post primary production process, void replacement is essential to success so the solvents should present in the gaseous phase at reservoir conditions. The solvents should have good solubility and favorable economics. CO_2 and CH_4 have been identified as the stable carrier gases and C_3H_8 is used to enrich the injected gas (Alvarez et al., 2014).

2.3.2 Experimental Study of CSI

Several CSI experiments were conducted during the past 20 years. Many researchers such as: Lim et al. (1995), Cuthiell et al. (2006), Jamaloei et al. (2012), Ivory et al. (2012), Qazvini Firouz and Torabi (2012), Du et al. (2015) operated laboratory experiments to investigate the performance of solvent based cyclic production in unconsolidated reservoirs. Three stages of CSI process that an injection process of solvent, followed by a soaking period and a production process were taken into consideration. Lim et al. (1995) studied the cyclic stimulation of cold lake oil sand with

supercritical ethane. Their experiments were employed in a 3-D physical model with a net confing pressure of approximately 1500 kPa on the model. The oil recovery factor, oil production rate, producing gas oil ratio and the solvent replacement ratio were presented and analyzed to examine the effect of the supercritical ethane. They observed that the supercritical ethane can extract a great number of heavy oil fractions than the sub-critical ethane. The oil recovery factor was higher while the production quality was lower for the supercritical ethane injection. Ivory et al. (2010) conducted an experiment using solvent mixture with 28% C_3H_8 and 72% CO_2 in the post-CHOPS follow-up process. Their experiments consisted of primary production followed by 6 cycles of CSI, with the physical model configured in a vertical alignment with a narrow end down. After 6 cycles production, 40% oil recovery was achieved, which indicated the potential of CSI process in post-CHOPS production. Qazvini et al. (2012) conducted a series of core experiments vertically placed in a core holder. In their study, CO_2, CH_4, C_3H_8 and C_4H_{10} were tested under different conditions. What they have observed that the CO_2 huff-n-puff approach was more efficient than methane-based solvents, and they also investigated the impact of different solvent compositions that CO_2-C_3H_8 and CO_2-C_4H_8 solvent mixtures had the potential of producing more oil than pure CO_2 case. In addition, they found that longer soaking time had more effect on cyclic solvent injection when operating at higher pressure. Ahadi and Torabi (2018) performed series of huff-n-puff tests under different operating pressures and hydrocarbon concentrations on heavy oil samples with viscosity of 1850 mPa·s to investigate the optimal solvent concentrations. They have observed that higher concentration of propane in the solvent mixture contributed to more oil production while methane exhibited an opposite trend that higher concentration in CH_4 and CO_2 solvent reduced the oil production. Jia et al. (2015) proposed a new CSI approach, in which the gas flooding-assisted cyclic solvent injection (GA-CSI) was considered to enhance oil recovery. A series of

experimental tests were conducted in two types of physical models: two cylindrical and one rectangular model). Foamy oil characteristic was also incorporated in the model during the pressure drawdown process. Their results illustrated that the oil production rate of the newly proposed GA-CSI process is three or four times of that in conventional CSI process. Besides, the impacts of the wormhole generated during the primary production on post-CHOPS oil production were investigated by Du et al. (2015). Their experiments suggested that the wormhole coverage has a significant effect on the CSI performance, which means that better CSI performance rom larger wormhole overage. These observations were beneficial for better understanding the impacts of wormholes on CSI process.

2.3.3 Numerical Study of CSI

Foamy oil is not only encountered during primary CHOPS production through evolving methane originally in oil but also applied in post-CHOPS processes by cyclically injecting different types of solvents. In the past few years, several numerical simulation studies were conducted to match their laboratory experimental results. Ivory et al. (2010) created a numerical CSI approach to match their radial drainage experiments. They defined three oil phase components and one gas phase component in the CSI model to simulate the condition at the end of the primary production. CMG-STARS simulator was used and foamy oil kinetic reactions were defined to mimic the non-equilibrium processes: gas dissolution, bubble gas nucleation and gas exsolution. They incorporated the non-equilibrium properties such as: solvent solubility, solvent and oil viscosity mixing rule and dispersion and diffusion coefficients into the reservoir model. They also conducted the parametric study in terms of K-values, capillary pressure and relative permeabilities, which indicated that the oil production was highly dependent on the kinetic reaction rates of the solvent dissolution and exsolution during the solvents injection and production processes. Chang and Ivory

(2013) conducted another CSI study on an avenue to optimize the CSI parameters in the field scale and showed the predictions of post-CHOPS reservoir characterizations. The CSI model was built on the basis of their previous study (Ivory et al., 2010) with the wormholes network region. They compared the oil production in different wormhole regions, which included an effective high permeability zone, a dual-permeability zone, a dilated zone and the wormholes extending from the well without the branching as well as the wormholes extending from the well with the branching (Spokes and branches model). The solvent mixture they used in the study consist of 60% methane and 40% propane, and the impacts of gas dissolution and gas exsolution reaction constants, injection strategies, grid size and upscaling were studied. Their observations indicated that the assumption of the equilibrium solubility condition resulted in reducing the oil production compared to the non-equilibrium solubility behavior. They also presented that higher oil production was achieved in the effective permeability non-equilibrium case. Therefore the wormhole network caused greater contact area for solvents penetrating during CSI in the field cases. In addition to that, Zhang et al. (2016) investigated the uncertainty of upscaling the post-CHOPS reservoirs. Six CSI cycles were incorporated into the simulation model on the basis of the experimental study published by Du et al. (2014). The key parameters such as foamy oil kinetic reaction rate constants, relative permeability, dispersion coefficients and capillary pressure were tune to do the history matching. Their sensitivity analysis indicated that capillary pressure influenced most during the upscaling of CSI model, which exhibited that the larger physical model, smaller capillary pressure were needed. The multilateral model replicated the wormholes generated in the CHOPS model and history matched the post-CHOPS oil and water production. Their CSI performance produced additional oil recovery in the range of 13-16% of the remaining oil in the reservoir. Hong et al. (2017) investigated the characteristics of the gas-oil flow in CSI.

Numerical simulation was conducted to history match seven lab-scale CSI tests under different pressure depletion rates.

Chapter 3. Description of Laboratory Data

3.1 Overview of Pressure Depletion Experiments

Pressure depletion tests were set-up in both bulk fluid systems and porous media to study the non-equilibrium release of solvent. Low field nuclear magnetic resonance (NMR) relaxometry was used to measure the dynamic live oil viscosity. The bulk fluid depletion set-up consists of the peek piston cylinder, mixer, and depletion pump (ISCO pump). The peek piston cylinder, which was made of the high-performance plastic and filled with pressurized live oil, could withstand high pressure (controlled by the ISCO pump) without interfering with the NMR signals. For the sand pack depletion set-up, the ISCO pump was used to control the fluid discharges (i.e., cumulative gas and liquid production volumes). Details of the experimental studies can be found in Bryan *et al.*, 2018. For the sake of completeness, the following sections are presented to offer a summary of the experimental procedures and data collected, which will be used in the modeling study described in Chapter 4 and 5.

3.2 Experimental Materials

3.2.1 Dead Oil Preparation

The heavy oil samples were extracted from oil emulsion samples provided by an Alberta CHOPS producer. The oil emulsion samples were cleaned by spinning for four hours at 10,000 rpm and 25 ^{o}C in a Beckman Ultracentrifuge. The residual water cut was estimated from NMR measurements, ensuring that the oil used in this study would contain <10% emulsified water for accurate dead oil

viscosity measurement, which was conducted at six different temperatures using the Brookfield Cone-Plate Viscometer. NMR measurement was also conducted at the same temperatures, in order to establish a reliable correlation between dead oil viscosity and average NMR relaxation time. **Table 3.1 and 3.2** summarize the dead oil properties and the viscosity measurements at different temperatures, respectively. At the test depletion temperature (25 °C) dead oil has a viscosity of 3370 mPas.

Table 3. 1 Properties of dead oil at 25 °C (Bryan *et al.*, 2018).

Temperature （°C）	Density (g/cm^3)	API Gravity	Water Cut (wt%)
15.6	0.9753	13.58	4.030

Table 3. 2 Dead oil cone-plate viscosity at six different temperatures (Bryan *et al.*, 2018).

Temperature (°C)	15.6	20	25	40	60	80
Viscosity (mPa·s)	8388	5464	3370	1055	301	113

3.2.2 Live Oil Preparation

Three solvent compositions were used (see below).

(1) Solvent 1: 35% CO_2 and 65% CH_4;

(2) Solvent 2: 80% CO_2 and 20% CH_4;

(3) Solvent 3: 35% C_3H_8 and 65% CH_4.

Table 3.3 and **Table 3.4** show the conditions and viscosities of the saturated live oil at 20 °C and 25 °C, respectively. The density of live oil-solvent 1 at 1600 kPag and 20 °C was 0.9561 g/cm^3, which was similar to the dead oil density of 0.9696 g/cm^3 at 20 °C. While data was initially

measured at 20 ºC (Table 3.3) the depletions were eventually run at 25 ºC so all viscosity and saturated oil GOR values were also measured at this temperature (Table 3.4).

Table 3. 3 Properties of one live oil sample at 20 ºC at different saturation pressures (Bryan *et al.*, 2018).

Live oil state	Saturation pressure, kPag	GOR, cm^3/cm^3	Viscosity, mPa·s
Live oil-Solvent 1 ($35\%CO_2/65\%CH_4$)	690	2.5	5004
	1240	4.5	3906
	1600	6.9	3300

Table 3. 4 Properties of three live oil samples at 25 ºC and different saturation pressures (Bryan *et al.*, 2018).

Live oil state	Saturation pressure, kPag	GOR, cm^3/cm^3	Viscosity, mPa·s
Live oil-Solvent 1 ($35\%CO_2/65\%CH_4$)	1600	6.9	2150
Live oil-Solvent 2 ($80\%CO_2/20\%CH_4$)	1600	11.0	1370
Live oil-Solvent 3 ($35\%C_3H_8/65\%CH_4$)	690	2.5	2900
	1240	4.5	2790
	1600	9.2	1450

3.3 Sand Pack Preparation

The sand pack was prepared using Lane Mountain 70 silica sand, and its properties are presented in **Table 3.5**. It was an unconsolidated system with no overburden stress. Porosity and absolute permeability were obtained through gas expansion and brine saturation. The core was saturated with water initially and subsequently flooded with oil. The core flooding experiment is described

in **Table 3.6**. At the end of the water flooding and oil flooding states, relative permeabilities for the water and oil phases are measured, and the results are shown in **Table 3.7**.

Table 3. 5 Core properties (Bryan *et al.*, 2018).

Core diameter (cm)	3.785
Core area (cm^2)	11.25
Core length (cm)	15.08
Core volume (cm^3)	169.7
Gas expansion PV (cm^3)	78.5
Gas expansion porosity (fraction)	0.463
Brine saturation PV (cm^3)	75.8
Initial water saturation (fraction)	0.966
Initial void space saturation (fraction)	0.034
Initial core density (kg/m^3)	1870

Table 3. 6 Results of core flooding with live oil at initial condition of 1600 kPag (Bryan *et al.*, 2018).

Total PV injected	3.035
Live oil in the core (g)	64.64
Live oil in the core (cm^3)	67.61
Water in the core prior to oil injection (cm^3)	7.28
S_o (fraction)	0.891
S_w (fraction)	0.096
Final producing GOR (cm^3/cm^3)	5.69

Table 3. 7 End point permeability and fluid saturations at initial condition of 1600 kPag (Bryan *et al.*, 2018).

Fluid state	S_o	S_w	S_g	Measured Permeability (mD)	Relative permeability
Water-saturated	0	0.966	0.034	4890	1 (water)
Live oil-saturated	0.891	0.096	0.013	4190	0.857 (oil)

3.3 Experimental Procedures

3.3.1 Live Oil Depletion in Bulk Fluid Systems

The saturated live oil in the mixer was further pressurized to an undersaturated condition at 1800 kPag, which was higher than the saturation (mixing) pressure of 1600 kPag. The PEEK vessel was filled with live oil at this pressure and then connected to the production ISCO pump to control the pressure depletion rate. NMR measurements were collected throughout the entire depletion process. Two depletion rates at 130 kPa/h (fast depletion) and 12.5 kPa/h (slow depletion) from 1800 kPag to 140 kPag were tested using all three solvents, in order to investigate the impact of depletion schedule on non-equilibrium foamy oil viscosity response. Solvents 1 and 2 have the same solvent components (i.e. CO_2 and CH_4) but with different compositions, so their solution GOR and live oil viscosity values are different. Solvent 3 has a similar viscosity to Solvent 2, but with a different solvent composition (i.e. C_3H_8 instead of CO_2). For the depletion in the sand pack, only the live oil saturated with Solvent 3 was used, at the slow depletion rate. Descriptions of the bulk fluid and sand pack depletion tests are summarized in Table 3.8.

Table 3. 8 Description of depletion tests (Bryan *et al.*, 2018).

Medium	Solvent type	Solvent Composition	Depletion Rate (kPa/h)	Depletion Scheme
Bulk fluid system	Solvent 1	35%CO_2/65%CH_4	Slow depletion:12.5	**Stage I**: Pressure decline from 1800 kPag to 140 kPag. **Stage II**: Constant pressure at 140 kPag for 80 hours.
			Fast depletion:130	
	Solvent 2	80%CO_2/20%CH_4	Fast depletion:130	
	Solvent 3	35%C_3H_8/65%CH_4	Slow depletion:12.5	
			Fast depletion:130	
Porous media	Solvent 3	35%C_3H_8/65%CH_4	Slow depletion:12.5	**Stage I**: Pressure decline from 1800 kPag to 200 kPag **Stage II**: Constant pressure at 200 kPag for 4.8 days **Stage III**: Pressure decline from 200 kPag to atmospheric condition over for a period of 3 days

3.3.2 Foamy Oil Viscosity Measurement Using NMR Relaxometry

NMR relaxometry entails excitation of the protons and measuring the subsequent relaxation time (Coates *et al*, 1999). In principles, viscous liquids that are bound in small cages would release the energy quickly, giving rise to short relaxation time; on the contrary, liquids with lower viscosity would release the energy slowly and be associated with longer relaxation time. NMR relaxometry can be applied to measure the "intrinsic viscosity", which reflects how tightly the liquid molecules are bound to the "cages". Viscosity was estimated based on the geometric mean of the T_2 distribution (T_{2gm}) utilizing the correlation established previously between the dead oil viscosity and T_{2gm} (Butron *et al*, 2016).

Chapter 4. Simulation Models

4.1 Fluid Model

The fluid model is characterized using the Peng-Robinson Equation of State (WinProp User Guide, 2016). A pseudo-component called "dead oil" was defined by specifying any two of the three parameters: MW (Molecular Weight), SG (Specific Gravity), and T_b (Normal Boiling Point). A SG value of 0.975 was computed directly from the measured API gravity value of 13.58. It was further assumed that the MW was 450 g/mole (Wang *et al*., 2015; Yadali *et al.*, 2012). The Twu (Twu *et al*., 1991) and Lee-Kesler correlations (Lee and Kesler, 1975) were used to determine a set of initial estimates of the critical temperature (T_c), critical pressure (P_c), and acentric factor (ω) of the dead oil component; these correlations are generally recommended for systems involving the Athabasca, Wabasca, Peace river and Cold Lake bitumen with different solvents (Kariznovi *et al*., 2009). The Pedersen Corresponding State Model (Pedersen and Fredenslund , 1987) was used to predict the liquid viscosity. Feed mole fractions are calculated from the GOR, and the calculated values for the three live oil systems are listed in **Table 4.1**. Detailed calculation procedure is described in section 4.1.1.

Table 4. 1: Calculated Feed Mole Fractions of Primary Component (Dead Oil) from GOR

Live oil state	Temperature (℃)	Pressure (kPag)	GOR (cm^3/cm^3)	Calculated Primary (Dead oil) Feed Mole Fraction
Live oil-Solvent 1 35%CO2/65%CH4	20	690	2.5	0.963
		1240	4.5	0.895
		1600	6.9	0.815
	25	1600	6.9	0.817
Live oil-Solvent 2 80%CO2/20%CH4	25	1600	11	0.737
Live oil-Solvent 3 35%C3H8/65%CH4	25	690	2.5	0.964
		1240	4.5	0.897
		1600	9.2	0.770

4.1.1 Calculation of Feed Mole Fraction Number

The feed primary mole fraction can be calculated from the given GOR data. Gas Oil Ratio (GOR, cm^3/cm^3) can be expressed as:

$$GOR = \frac{V_g}{V_o} \tag{4-1}$$

Where V_g represents the total dissolved gas volume and V_o represents the oil volume at a specific condition. In order to get the mole fraction number of oil and gas, the average molar mass of the gas mixture should be calculated first. Average molar mass of the gas mixture can be computed through Equation 4-2 (Janet, 2016):

$$M_{Avg} = \sum_{i=1}^{n} M_i P_i \tag{4-2}$$

Where M_{Avg} (g/mole) denotes the average molecular weight of the solvent mixture, i is the index of each gas component, n is the total number of gas components in the mixture, M_i (g/mole) is the molecular weight of gas i and P_i represents the molar percentage of gas i in the mixture. For

instance, the solvent 3 consists of 65% CH_4 and 35% C_3H_8 in the mixture, and the average molar mass following the above equation after calculation is 25.8 g/mole. Next, based on the Ideal Gas Law (Wikipedia., 2019), the density of the solvent mixture can be calculated by Equation 4-3:

$$PV = nRT \tag{4-3}$$

Based on Ideal Gas Law equation, the density of gas solvents mixture can be obtained from Equation 4-4:

$$\rho = \frac{PM}{RT} \tag{4-4}$$

Where P (kPa) is the absolute pressure of gas, V (cm^3) is the volume of gas, n represents the gas mole numbers, R is the ideal or universal gas constant, which equals to 0.08206 L·atm/(mol·K) (convert the unit to cm^3·kPa/(mol·K), R=8.28806×10^4 cm^3·kPa/(mol·K)). T (K) is the absolute gas temperature and ρ (g/cm^3) is the gas density. It should be noted that the calibrated experimental pressure is the "Gauge Pressure" (kPag), which should be converted to the absolute pressure (kPa). The gauge pressure equals to the absolute pressure minus the atmosphere pressure (Engineering Toolbox., 2014). Then, calculate the mass ratio of solution gas and dead oil. Here, assuming the dead oil is incompressible liquid with a constant density at a fixed temperature and different pressures.

$$\frac{m_g/\rho_g}{m_o/\rho_o} = \frac{V_g}{V_o} = GOR \tag{4-5}$$

$$\frac{m_g}{m_o} = \frac{\rho_g * GOR}{\rho_o} \tag{4-6}$$

Where m_g and m_o are mass of gas and oil, ρ_g (g/cm^3) and ρ_o (g/cm^3) are density of gas and oil. The ratio of gas and oil mole numbers is calculated from Equation 4-7:

$$\frac{n_g}{n_o} = \frac{m_g/M_g}{m_o/M_o} \tag{4-7}$$

$$n_g + n_o = 1 \quad (4\text{-}8)$$

Where n_g and n_o represent gas and oil mole numbers, M_g and M_o are the molecular weight of gas and oil. Combing equations 4-9 and 4-10, the feed mole fraction number of primary component (dead oil) " n_o" can be computed. Final calculation results of primary component (dead oil) feed mole fraction numbers are shown in **Table 4.1.**

4.1.2 Fluid Modeling Results

The saturation pressure data in **Table 3.4** was used to tune T_c, P_c, ω, volume shift factor, and interaction coefficients, while viscosity measurements in **Tables 3.2 to 3.4** are used to adjust the viscosity coefficients in the Pedersen model, for the dead oil component. Comparison between the lab measurements and fluid model predictions are shown in **Figure 4.1** and **Figure 4.2**. The match is acceptable, considering that most properties of the pseudo-component, "dead oil", are missing; a more thorough characterization of the dead oil would help to reduce this mismatch. In addition, as the fluid model should capture all the PVT properties of three live oil-solvent systems together into the WinProp in terms of saturation pressures, dead oil and live oil viscosities (Table 3.3 and 3.4), it is more difficult and challenging to tune and match with experimental data, after tuning the regression parameters for many times, although the fluid simulation results cannot achieve perfectly matching, the results are reasonable and acceptable. Results for the live oil-solvent 2 system are not shown here graphically because there was only a single saturation pressure measured, and predicted value of 1577 kPag is very close to the measured value of 1600 kPag; the corresponding predicted viscosity of 1152 mPa·s is also similar to the lab measurement of 1370 mPa·s. In addition, live oil viscosity increases as pressure decreases at equilibrium.

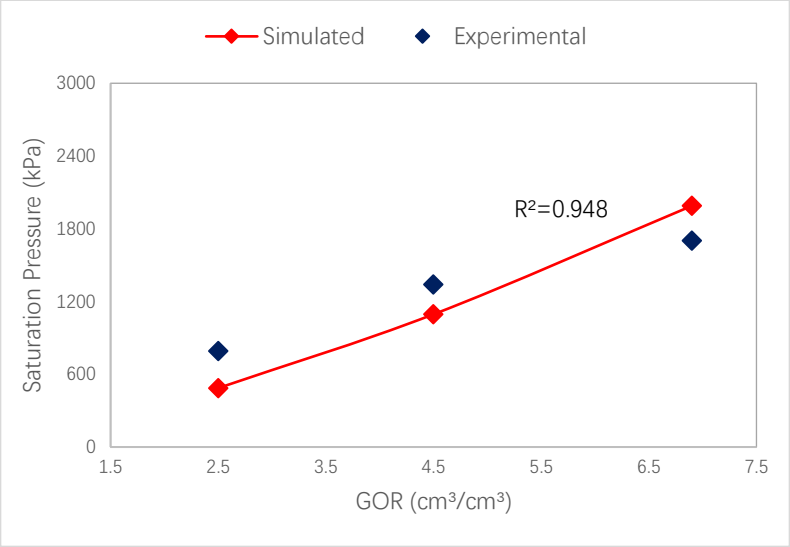

(a)

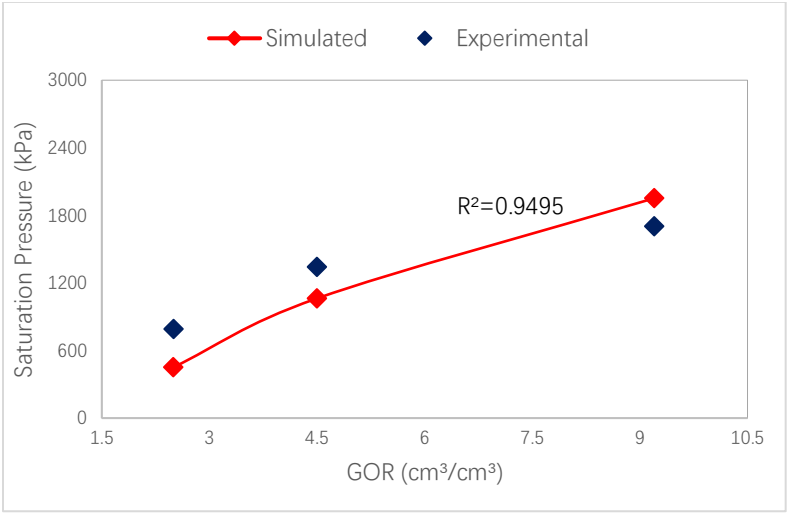

(b)

Figure 4. 1: Comparison between predicted and measured saturation pressure vs. GOR (from Table 3.4): (a) Live oil-Solvent 1 system with different primary feed mole fraction at 20 °C; (b) Live oil-Solvent 3 system with different primary feed mole fraction at 25 °C.

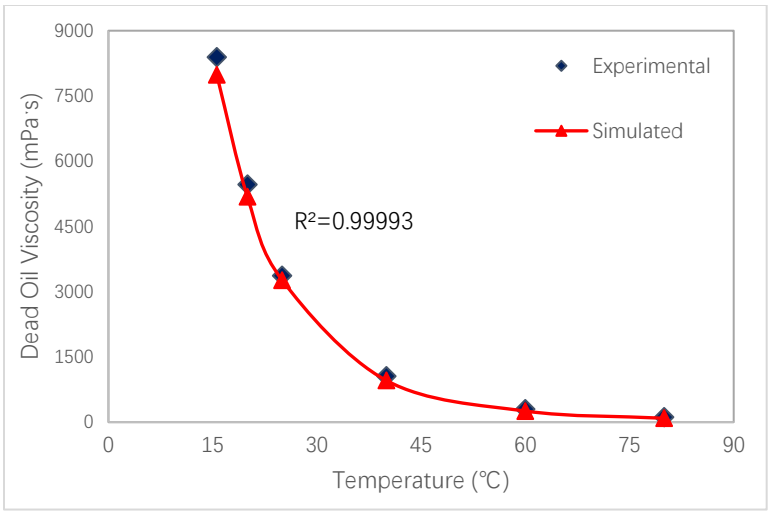

(a)

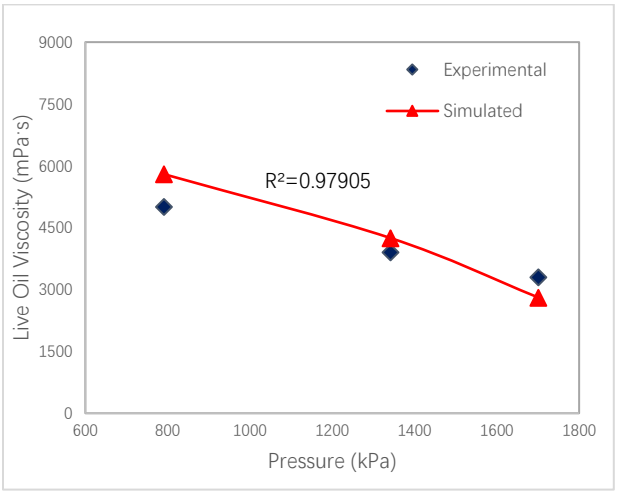

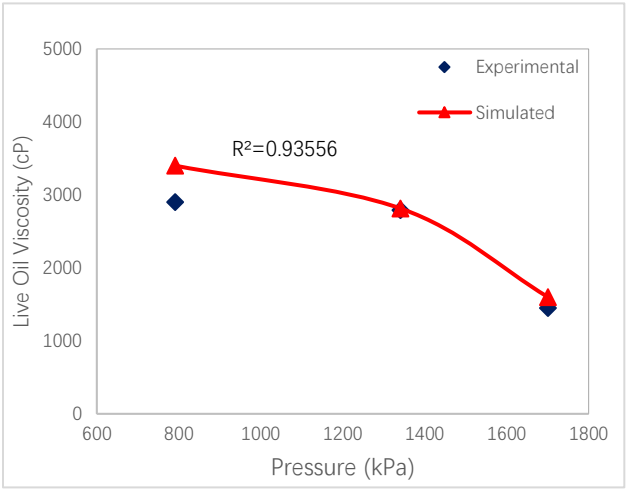

(b) **(c)**

Figure 4. 2: Fluid modeling results – comparison between model predictions and experimental data (a) dead oil viscosity (data from Table 3.2); (b) live oil viscosity of live oil-solvent 1 system at 20°C (data from Table 3.3); (c) live oil viscosity of live oil-solvent 3 system at 25 °C (data from Table 3.4).

Parameters of the tuned fluid model are summarized in **Table 4.2**. The tuned fluid model is used to construct numerical simulations of the sand-pack and field depletion processes. The equilibrium K values for each component are computed from the tuned PR-EOS model according to the following equation (Ivory et al., 2010):

$$K = (\frac{kv_1}{P} + kv_2 \times P + kv_3) \times \exp(\frac{kv_4}{(T - kv_5}) \quad (4\text{-}9)$$

Where *P, T* are pressure (kPa) and temperature ($°K$), respectively, and kv_1, kv_2, kv_3, kv_4 and kv_5 are the coefficients for the specific solvent component.

Table 4. 2: Tuned fluid model: dead oil and three solvents (CH_4, C_3H_8 and CO_2) components.

Component Name	Dead Oil	CO_2	CH_4	C_3H_8
Molecular Weight	450	44.01	16.043	44.097
Critical Pressure (atm)	8.45	72.8	45.4	41.9
Critical Temperature (K)	556	304.2	190.6	369.8
SG (Specific gravity)	0.975	0.818	0.3	0.507
Tb (Normal boiling point in ℃)	530	-78.45	-161.45	-45.05
Acentric Factor	1.1073	0.225	0.008	0.152
Hydrocarbon Binary Coefficient	1	3	1	1
Volume Shift	0.266	0	0	0
Volume shift temperature coefficient (1/℃)	0	0	0	0
Volume shift reference temperature (℃)	15.556	15.556	15.556	15.556
Z (Rackett) Factor	0.2397	0.2736	0.2876	0.2763
Vc Critical volume (l/mol)	1.456	0.094	0.094	0.203
Omega A	0.4572	0.4572	0.4572	0.4572
Omega B	0.0778	0.0778	0.0778	0.0778
Parachor	996.6	78	77	150.3

4.2 Simulation of Depletion Test in Sand Pack

4.2.1 Model Description

The simulation was performed using a thermal compositional simulator, STARS (CMG 2016). A 2D model is constructed to model the depletion in sand pack experiments. The cylindrical sand pack is approximated with a fine Cartesian mesh of 20 × 5 × 5 grid blocks along the x-, y-, and z-directions, representing the physical dimensions of 11.08 cm in length and 3.9135 cm in width and thickness. To model the pressure depletion process, a producer (single point source located at the center of the outlet face) is simulated, and the well bottom-hole pressure is reduced gradually from 1800 kPag. Other relevant model parameters are described in **Table 4.3**. Water-oil and gas-liquid relative permeability relationships are adopted from a previous study (Martinez Gamboa and Leung, 2019), as shown in **Figure 4.3**. The water-oil relative permeability functions (Figure 3.3a) correspond a water-wet system. For the gas-liquid relative permeability functions (Figure 3.3b), a reduced gas relative permeability end point and higher irreducible gas saturation is used to model the delay of free gas flow due to the non-equilibrium gas exsolution process. This modeling strartegy is often referred to as the modified fractional flow approach (Maini, 2001). It should be emphasized that the relative permeability functions are not tuned and remain unchanged, only the kinetic model parameters (section 3.2.2) are adjusted to match the sand-pack depletion experiments.

Table 4. 3: Reservoir properties for the sand-pack model

Property	value
Sand-pack length (cm)	11.08
Sand-pack width (cm)	3.9
Sand-pack height (cm)	3.9
Sand-pack volume (cm^3)	170
Porosity	0.46
Horizontal permeability (md)	4890
Vertical permeability (md)	4890
Rock compressibility (Pa^{-1})	2×10^{-5}
Initial reservoir pressure (kPag)	1800
Initial reservoir temperature (℃)	25
Initial oil saturation (fraction)	0.891
Initial gas saturation (fraction)	0.013
Initial water saturation (fraction)	0.096

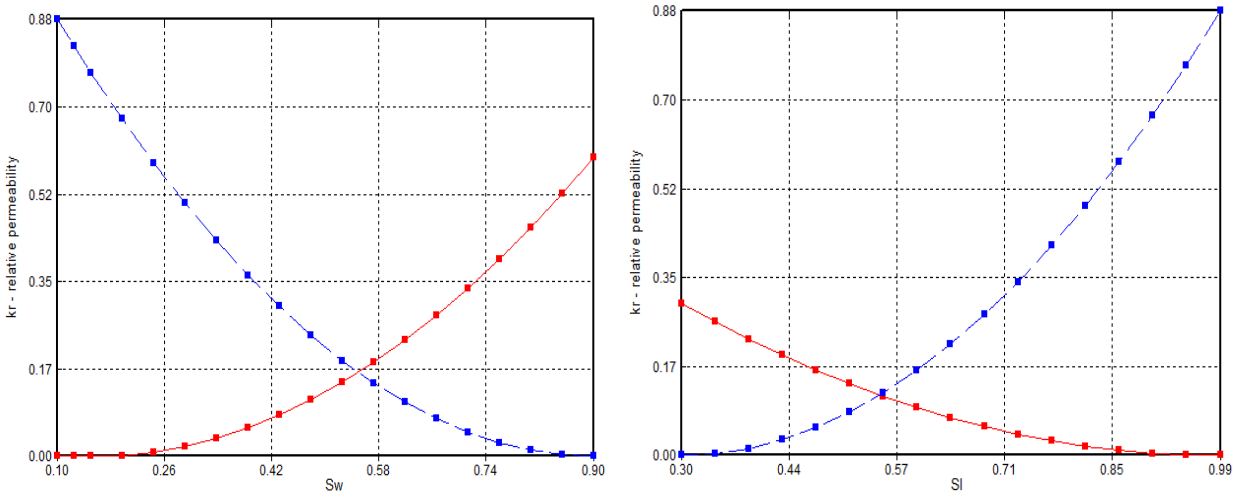

(a) **(b)**

Figure 4. 3: (a) Water-oil [red: water; blue: oil] and (b) gas-liquid [red: gas; blue: liquid] relative permeability functions

4.2.2 Foamy Oil Kinetic Reaction Model

The non-equilibrium process of foamy oil flow in a porous medium involves several stages: bubble nucleation, bubble growth and bubble coalescence. A kinetic model is used to represent these different stages. A five-component kinetic model involving heavy oil, water, dissolved gas, dispersed gas bubbles in the oleic phase and connected gas bubbles in the gaseous phase is adopted (Uddin, 2005). For example, considering the case of Solvent 3 (35%C_3H_8/65%CH_4) as an example, the foamy oil kinetic model can be described by the following reactions:

Reaction 1 describes the bubble nucleation process: the liberation of dissolved gas to trapped gas:

Reaction 1:

$CH_4\ (L) \rightarrow CH_4\_Bub\ (L)$ (4-10)

$C_3H_8\ (L) \rightarrow C_3H_8\_Bub\ (L)$ (4-11)

Reaction 2 describes the bubble growth and coalescence processes: the liberation of dispersed gas bubbles to form a continuous gas phase:

Reaction 2:

$CH_4\_Bub\ (L) \rightarrow$ Free$_CH_4\ (G)$ (4-12)

$C_3H_8\_Bub\ (L) \rightarrow$ Free$_C_3H_8\ (G)$ (4-13)

Where $CH_4\ (L)$ is the dissolved methane in oil phase, $CH_4\_Bub\ (L)$ is the dispersed methane bubbles in oil phase, Free$_CH_4\ (G)$ is the coalesced methane free gas in gaseous phase; $C_3H_8\ (L)$ is the dissolved propane in oil phase, $C_3H_8\_Bub\ (L)$ is the dispersed propane bubbles in oil phase, Free$_C_3H_8\ (G)$ is the coalesced propane free gas in gaseous phase.

The kinetic model also known as reaction kinetics, determines the speed of reaction r_k (CMG-STARS User's Guide). The general expression is:

$$r_k = r_{rk} \cdot \exp(-E_{ak}/RT) \cdot \prod C_j^{N_j} \quad (4\text{-}14)$$

The parameter r_{rk} is a constant for the reaction of r_k; E_{ak} is the activation energy; R is the universal gas constant; T is the temperature; $\prod$ is the product operator; C_j and N_j refer to the molar concentration and order of the j^{th} component. If isothermal conditions are assumed, the term involving E_{ak} and T can be ignored, such that only a single reaction constant is to be defined (Yu and Leung, 2019). The values of r_{rk} are determined via history matching of the experimental NMR-derived liquid viscosity profiles. It should be noted that dispersed gas bubbles are assigned the same properties as their dissolved counterparts, except for their density, for which the option of "gas like liquid density" should be selected. With limited experimental measurements, same values of r_{rk} are assumed for all three solvent components.

4.2.3 Mechanisms of Cyclic Solvent Injection (CSI) Process

The aforementioned model provides satisfactory results for modeling many pressure depletion processes, where only the mechanism of solvent exsolution is relevant; however, in the case of CSI, where multiple cycles of injection and production are involved, both non-equilibrium solvent dissolution and exsolution processes must be considered. Therefore, an alternative non-equilibrium foamy oil kinetic model developed by AITF is also tested in this study (Chang and Ivory, 2011). The model incorporates a number of important mechanisms associated with the CSI process (e.g. non-equilibrium dissolution an exsolution, as well as gas expansion). It has been validated extensively with both laboratory and field scale historical data (Chang and Ivory, 2013). The model consists of the following two parts:

4.2.3.1 Gas Dissolution

$CH_4\ (G) + CH_4\ (L) \rightarrow 2\ CH_4\ (L)$ (4-15)

$C_3H_8\ (G) + C_3H_8\ (L) \rightarrow 2\ C_3H_8\ (L)$ (4-16)

$CO_2\ (G) + CO_2\ (L) \rightarrow 2\ CO_2\ (L)$ (4-17)

Where $CH_4\ (G)$, $C_3H_8\ (G)$ and $CO_2\ (G)$ are the injected methane, propane and carbon dioxide in gaseous phase; $CH_4\ (L)$, $C_3H_8\ (L)$ and $C_3H_8\ (L)$ are the dissolved methane, propane and carbon dioxide in oil phase. Due to the lack of detailed experimental data available to calibrate the corresponding rate constants, same assumed values are used for three solvent systems.

4.2.3.2 Gas Exsolution

Bubble nucleation process: the liberation of dissolved gas to trapped gas:

$CH_4\ (L) \rightarrow CH_4\_Bub\ (L)$ (4-18)

$C_3H_8\ (L) \rightarrow C_3H_8\_Bub\ (L)$ (4-19)

$CO_2\ (L) \rightarrow CO_2\_Bub\ (L)$ (4-20)

Bubble growth and coalescence processes: the liberation of dispersed gas bubbles to form a continuous gas phase:

$CH_4\_Bub\ (L) \rightarrow$ Free$_CH_4\ (G)$ (4-21)

$C_3H_8\_Bub\ (L) \rightarrow$ Free$_C_3H_8\ (G)$ (4-22)

$CO_2\_Bub\ (L) \rightarrow$ Free$_CO_2\ (G)$ (4-23)

Where $CH_4\ (L)$, $C_3H_8\ (L)$ and $C_3H_8\ (L)$ are the dissolved methane, propane and carbon dioxide in oil phase; CH_4_Bub, C_3H_8_Bub, CO_2_Bub are the dispersed gas bubbles in oil phase; Free$_CH_4\ (G)$, Free$_C_3H_8\ (G)$ and Free$_CO_2\ (G)$ are the coalesced free gas in gaseous phase.

In addition, the diffusion coefficients for three solvent components C_3H_8, CO_2 and CH_4 are set as 0.001 cm^2/s (Martinez Gamboa and Leung, 2019)

4.3 Sand Pack Simulation Results and Discussion

4.3.1 History Matching of Sand Pack Experimental Data

The live oil was obtained by combining the dead oil with Solvent 3 (65% CH_4 and 35% C_3H_8) at a saturation pressure of 1600 kPag, and the sand pack was saturated with live oil at 25 ^oC (water saturation is at the irreducible level) and pressurized to 1800 kPag prior to any depletion tests. Only the slow depletion test (12.5kPa/h) was conducted for the live oil-Solvent 3 system in the sand pack (**Table 3.8**). The experimental profiles of oil viscosity, pressure, fluid flow rates were used to adjust the values of r_k (as described in the previous section). Despite that detailed measurements of rock-fluid and fluid-fluid interactions were not available, the predicted liquid viscosity profiles, oil rate and oil recovery factor profiles are in reasonable agreement with the experimental data, as shown in **Figure 4.4**. The liquid viscosity only increases slightly as the pressure declines; low viscosity is maintained during most of the depletion process, implying that the non-equilibrium solvent release has contributed to foamy oil flow. It is also noted that as the pressure drops below the equilibrium bubble point pressure (1600 kPag), the dissolved gas is not released immediately, while free gas is formed at a much lower pressure. Approximately 17% of the oil is recovered after the first and second stages of depletion from 1800 kPag to 200 kPag. An additional ~10% of oil is recovered after depleting the system to the ambient condition for another 3 days; this incremental oil recovery can be attributed to the solution gas drive from the evolved free gas.

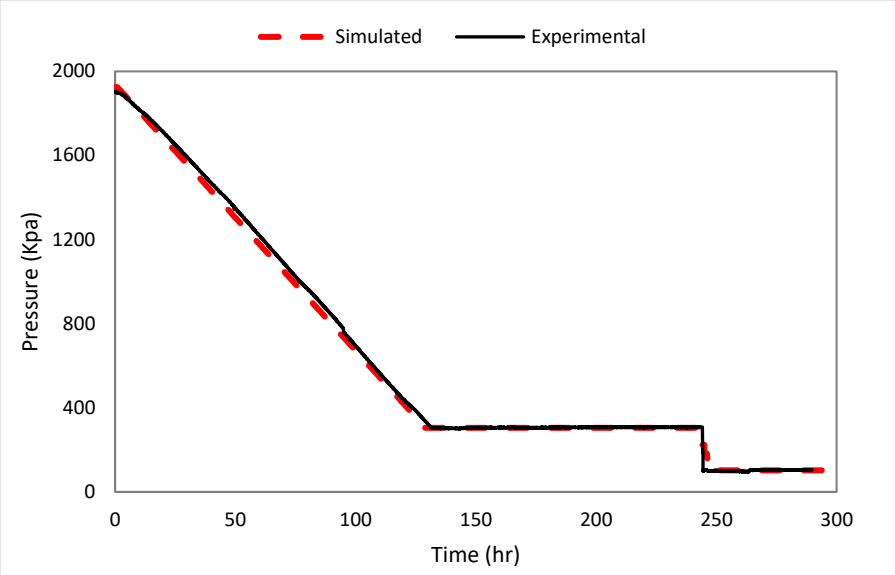
Simulated
Experimental
Pressure (Kpa)
2000
1600
1200
800
400
0
0
50
100
150
200
250
300
Time (hr)

(a)

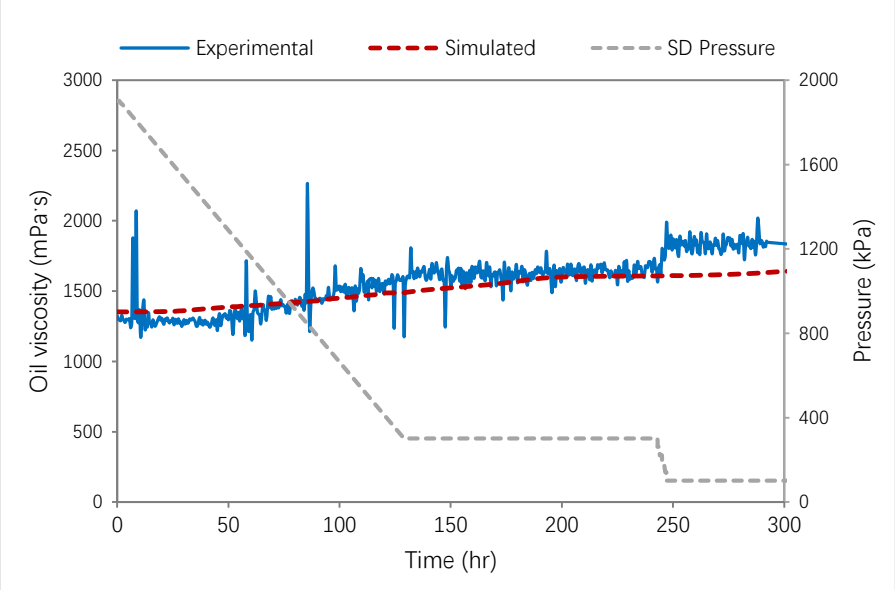
Experimental
Simulated
SD Pressure
Oil viscosity (mPa·s)
3000
2500
2000
1500
1000
500
0
Pressure (kPa)
2000
1600
1200
800
400
0
0
50
100
150
200
250
300
Time (hr)

(b)

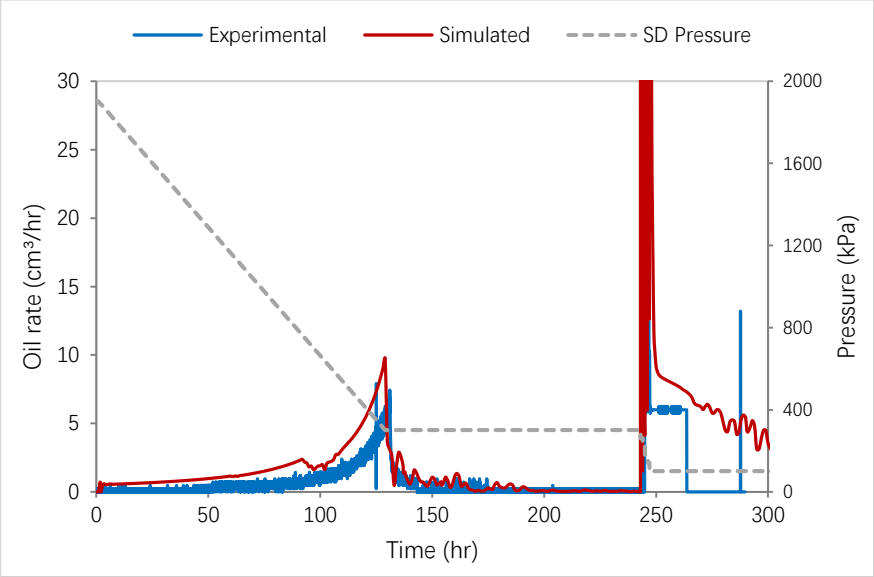

(c)

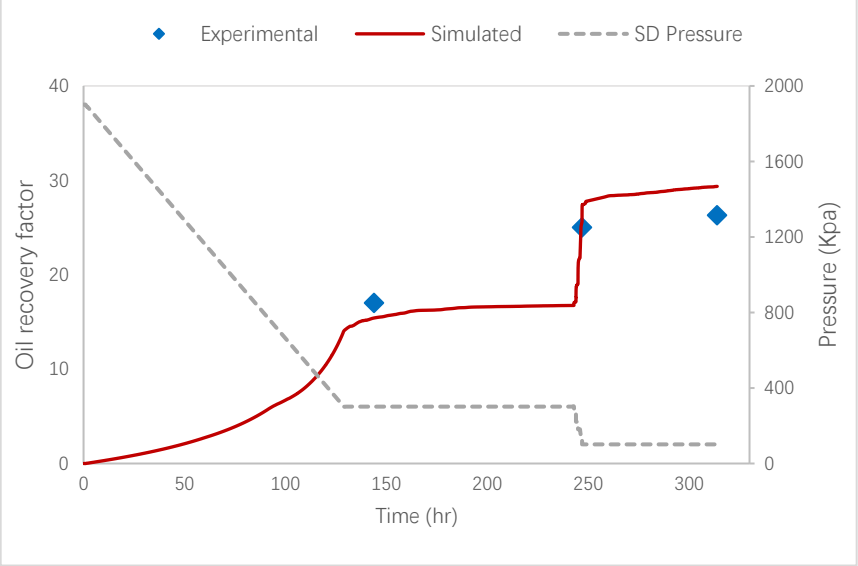

(d)

Figure 4. 4: History matching of sand pack experimental data involving Solvent 3: (a) differential pressure during slow depletion; (b) predicted and NMR-derived oil viscosity; (c) oil rate; (d) oil recovery.

4.4 Effects of Solvent Compositions and Pressure Depletion Rate

As shown in Table 3.8, viscosity profile in a sand pack was measured only for the case of SD using Solvent 3, and the results have been used in the previous section to history match the reaction kinetics (i.e., r_k). However, since no sand pack depletion experiments were performed for Solvents 1 and 2, the same reaction kinetics are also used for the CO_2 systems (i.e., Solvents 1 and 2). In fact, additional simulation models are constructed to predict the pressure depletion profile using all three solvent compositions with both FD and SD schemes.

4.4.1 General Characteristic of Foamy Oil Flow in the Sand Pack Model

Certain characteristics pertinent to foamy oil flow can be observed for all solvent types. For example, considering the live oil-solvent 2 system in **Figure 4.5**, three distinct stages during the depletion process can be identified (Sun et al., 2018). In the first stage, small volume of oil is produced at pressures above the pseudo-bubble point (P_b'), as small amount of dispersed gas bubbles exist and the oil production primarily results from expansion of the liquid phase (Tang and Firoozabadi, 2005). During the second stage, oil production rapidly increases (from 4% to 40%); foamy oil flow becomes more prominent, and large amount of dispersed gas bubbles are formed (Sun et al., 2018). The dispersed gas bubbles also swell the oil volume, providing additional drive for oil production and pressure maintenance. During the third (last) stage, the gas bubbles start to coalesce and become a continuous (free) gas phase; the critical gas saturation (S_{gc}) is attained, and given that the gas mobility is much higher than the oil mobility, a significant decrease in oil production is observed (Alshmakhy and Maini, 2012).

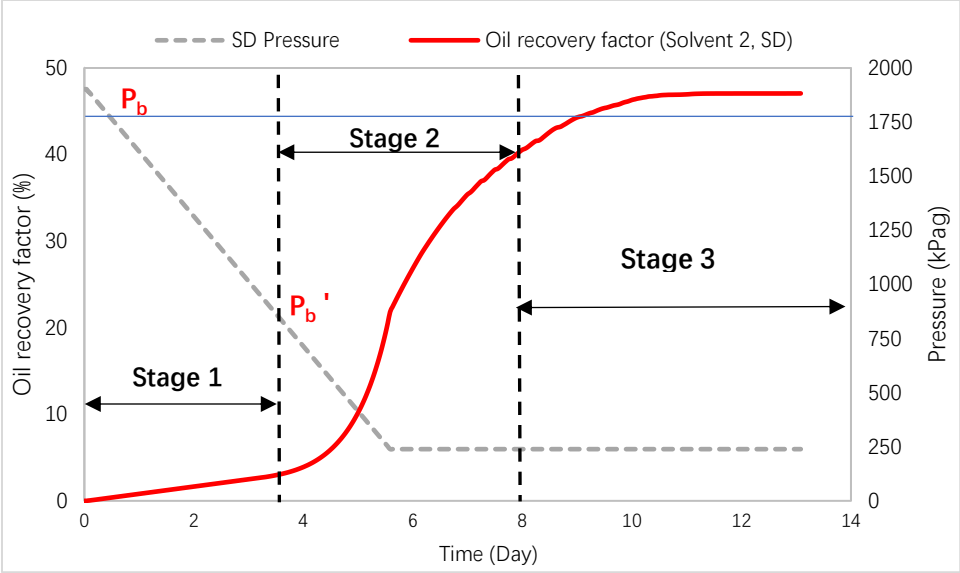

(a)

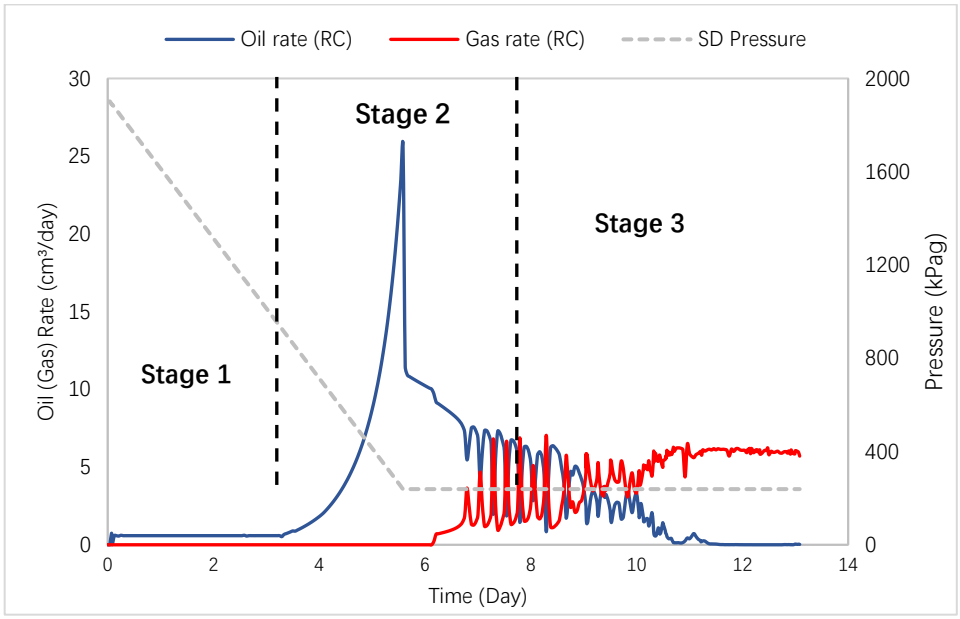

(b)

Figure 4. 5 Live oil-solvent 2 system under slow depletion: (a) oil recovery factor; (b) oil and gas rates.

4.4.2 Effects of Pressure Depletion Rate

Comparisons of the production performance under slow and fast depletion for all three solvents are shown in **Figure 4.6-4.8**. As discussed previously, depletion in a sand pack was conducted using only C_3H_8; therefore, no dynamic data can be used to tune the foamy oil kinetic parameters for the CO_2 solvent. As a result, the same kinetic parameters as Solvent 3 are used to model the foamy oil behavior for both C_3H_8- and CO_2-based systems, assuming that the rates of bubble formation and solvent exsolution are the same. The observed difference in the ensuing non-equilibrium solvent release is due to the difference in phase behavior between the heavy oil with C_3H_8 and CO_2. Comparing Figure 4.6 with Figure 4.8, it is noted that production profiles for Solvent 1 (35% CO_2) is similar (or only slightly higher) than those for Solvent 3 (35% C_3H_8), suggesting that assigning the same reaction kinetics to both C_3H_8 and CO_2 could be justified. In fact, this assumption would yield a more conservative estimate of CO_2 foamy oil behavior because recoveries for Solvent 1 is actually slightly better than those for Solvent 3. Both the bulk fluid system experiments and sand pack simulation results have illustrated that a higher oil production can be achieved under fast depletion, corroborating with other studies (Maini, 2001; Tang and Firoozabadi, 2005). It is likely that a higher pressure depletion rate would generate more nucleation sites and dispersed gas bubbles, enhancing the foamy oil behavior. Slow depletion leads to a significant delay in production due to reduced foamy oil flow (fewer dispersed gas bubbles). In the case of bulk system tests, despite of a production delay, the final recovered volumes are similar for both FD and SD. However, in the simulated sand pack results, the recoveries are lower under slow depletion. One plausible explanation is that the time scale for the sand pack test is much longer than the bulk system tests, so there is more time for the gas bubbles to become free gas

eventually. This explanation is corroborated by the lower recovered volumes from sand packs than in the bulk systems.

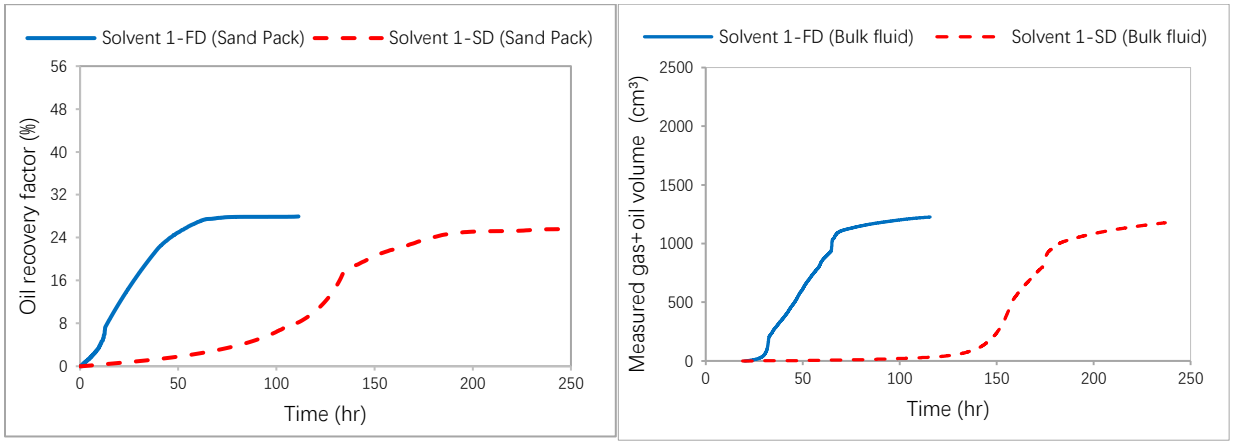

(a) **(b)**

Figure 4. 6 Results comparison for fast and slow depletions corresponding to Solvent 1: (a) sand pack simulation results of the oil recovery factor; (b) measured cumulative produced (oil+gas) volume from bulk fluid system experiments (Bryan *et al.*, 2018).

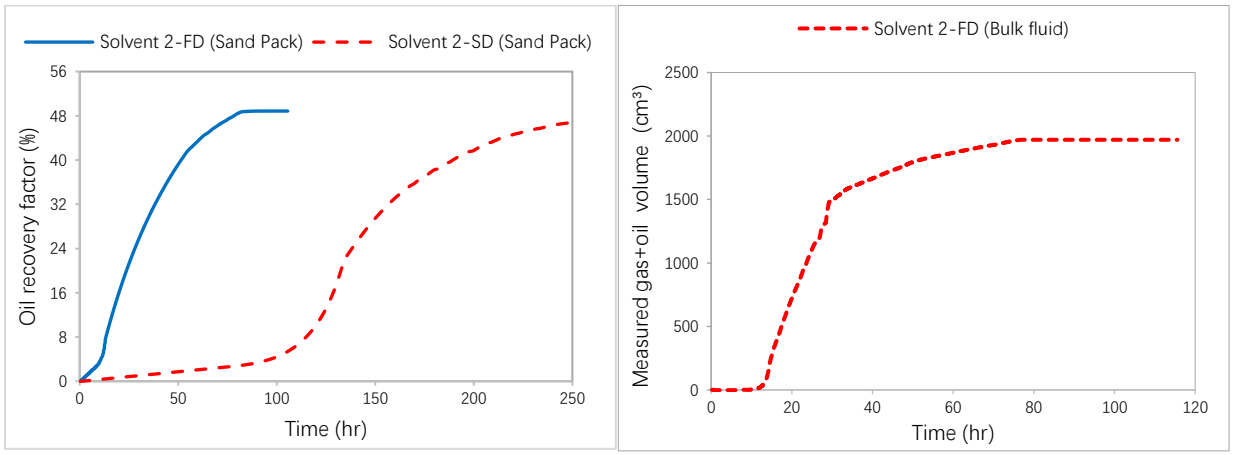

(a) **(b)**

Figure 4. 7: Results comparison for fast and slow depletions corresponding to Solvent 2. (a) Sand pack simulation results of the oil recovery factor; (b) measured cumulative produced (oil+gas) volume from bulk fluid system experiments (only fast depletion data was measured) (Bryan *et al.*, 2018).

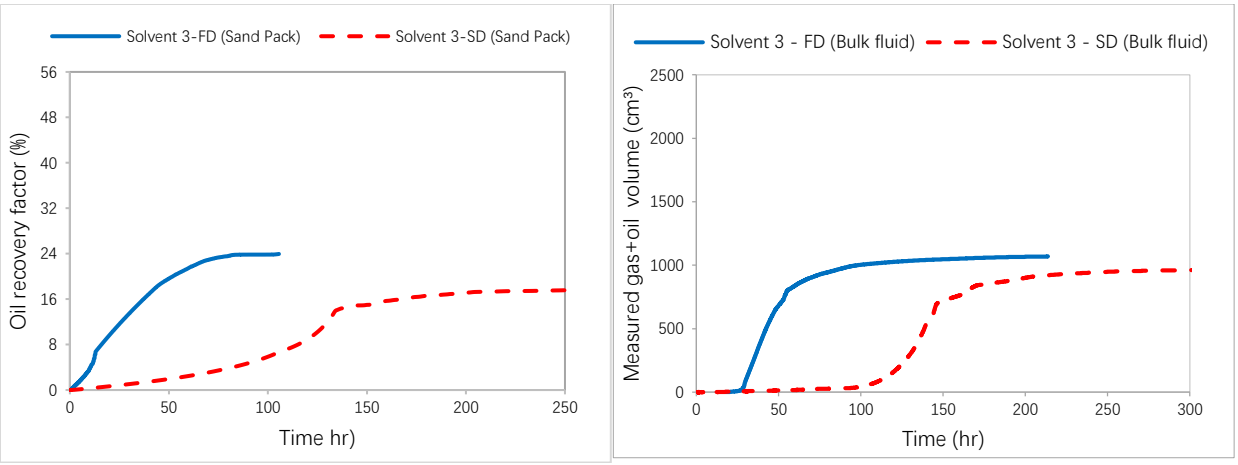

(a) **(b)**

Figure 4. 8 Results for fast and slow depletions corresponding to Solvent 3: (a) sand pack simulation predictions of oil recovery factor; (b) measured cumulative produced (oil+gas) volume from bulk fluid system experiments (Bryan *et al.*, 2018).

Figures 4.9-4.11 compare the amount of dispersed gas bubbles in the production stream during the fast and slow depletions. In Figure 4.9, for Solvent 1 system (65% CH_4 and 35% CO_2), both CH_4 and CO_2 are participating in the foamy oil kinetic reactions; there is a higher CH_4 content, so more CH_4 gas bubbles are detected. It is clear that FD generates more dispersed CH_4 and CO_2 gas bubbles, which is translated into increased foamy oil flow and oil production. Similar observations are noted in Figure 4.10, except that more CO_2 bubbles are detected for Solvent 2 (which consists of 80% CO_2). The high solubility of CO_2 compared to CH_4 is also shown in these figures: under FD there are no CO_2 bubbles until the system reaches the end point value (200 kPag) for both solvents 1 and 2. Under SD, even for the high CO_2-content in Solvent 2, CO_2 bubbles are not predicted until pressures that are less than 800 kPag. For Solvent 1 with low CO_2 content, the impact of CH_4 release enables CO_2 to stay in solution until the pressure has dropped to its final level of 200 kPag. For both solvents, there are fewer CH_4 and CO_2 bubbles under SD, as compared to FD, even long after the pressure has depleted down to 200 kPag; this is because the remaining CH_4 and CO_2 have already evolved as free gas. It should also be noted that for both solvents, the

amount of CO_2 released is also much less than the injection solvent composition, indicating that there is considerable retention of CO_2 in oil even at low pressures.

When comparing the results of C_3H_8 (Figure 4.11) against CO_2 (Figures 4.9 & 4.10), for Solvent 3, there is essentially no C_3H_8 bubbles due to the high solubility of C_3H_8 in oil even at low pressures (Zhou *et al.*, 2016). Although C_3H_8 may not contribute to the foamy oil flow, it is, however, effective for reducing the live oil viscosity, but less evolved gas has also resulted in a decrease in oil production. Comparing Figures 4.6-4.8 would reveal that higher oil production is achieved when using CO_2-based solvents (Solvents 1 and 2) instead of C_3H_8-based solvent (Solvent 3). This is because, even though C_3H_8 has a highest solubility of all three solvent vapour components (i.e. 35% C_3H_8 gives the lowest live oil viscosity even compared to higher CO_2-content in Solvent 2), C_3H_8 does not leave solution with the oil even at 200 kPag, so the only driving force for oil production is the pressure support from the methane solution gas drive. In the case of CO_2 (solvents 1 and 2), an increase in CO_2 concentration (80% CO_2 in Solvent 2) leads to higher oil recovery, in comparison to Solvent 1 (35% CO_2), under both fast and slow depletion tests. This finding is consistent with several previous studies (Zhou *et al.*, 2016; Bjorndalen *et al.*, 2012; Soh *et al.*, 2018; Bera and Babadagli, 2016), which show that propane yieled a good mixing with heavy oil, however the lower foaminess reduced the drive energy to produce oil. The largest amount of gas bubbles are generated using the Solvent 2 system under both fast and slow decline rates, as shown in Figures 4.9-4.11.

Finally, the oil viscosity profiles for all three solvents are compared in Figure 4.12; they all exhibit significant non-equilibrium foamy oil behavior. Viscosities in both fast and slow depletion cases have remained close to its initial value, while a slight increase is observed in the slow depletion case as pressure drops below 140 kPag. This observation is a crucial characteristic in heavy oil

solvent CSI operations: as pressure drops, solvent does not evolve out of solution following equilibrium relationships with pressure. Instead, there is a delay in solvent release, particularly for CO_2 and C_3H_8, and this keeps the oil viscosity close to the initial live oil value even as pressure drops to provide a driving force for flow of diluted oil.

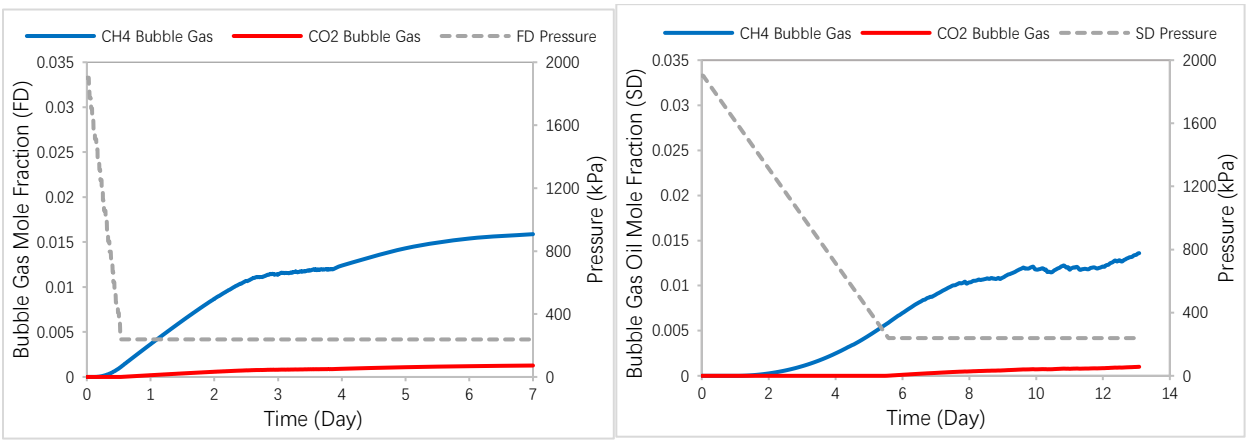

(a) **(b)**

Figure 4. 9: Live oil-Solvent 1 system: (a) CH_4 and CO_2 bubble gas mole fraction in the production stream during fast depletion; (b) CH_4 and CO_2 bubble gas mole fraction in the production stream during slow depletion.

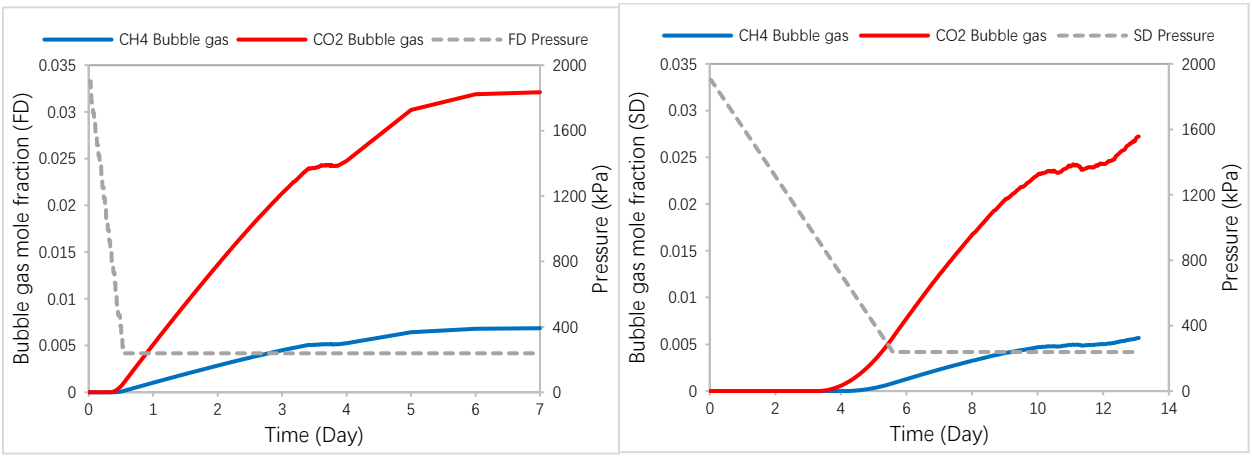

(a) **(b)**

Figure 4. 10: Live oil-Solvent 2 system: (a) CH_4 and CO_2 bubble gas mole fraction in the production stream during fast depletion; (b) CH_4 and CO_2 bubble gas mole fraction in the production stream during slow depletion.

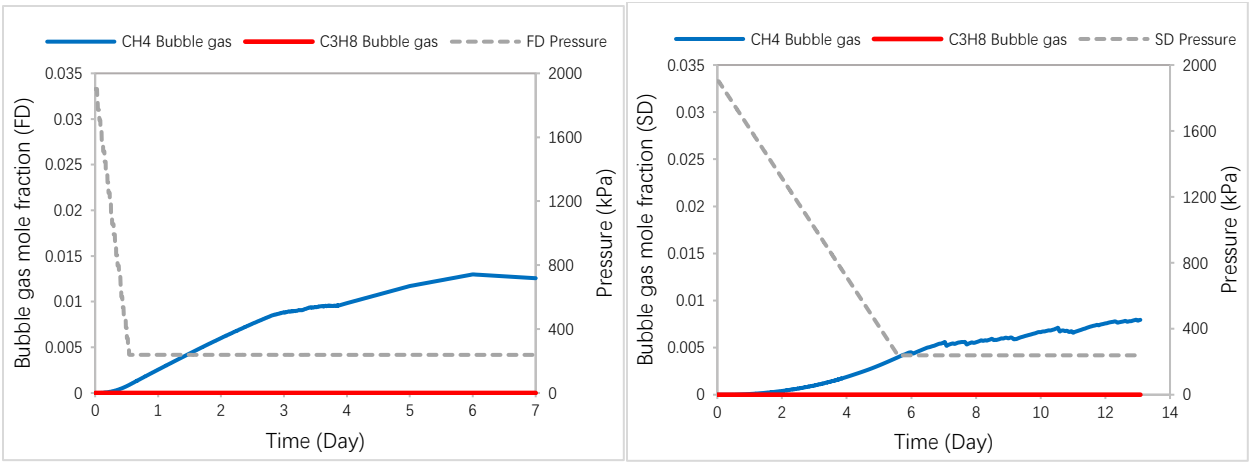

Figure 4. 11: Live oil-Solvent 3 system: (a) CH_4 and C_3H_8 bubble gas mole fraction in the production stream during fast depletion; (b) CH_4 and C_3H_8bubble gas mole fraction in the production stream during slow depletion.

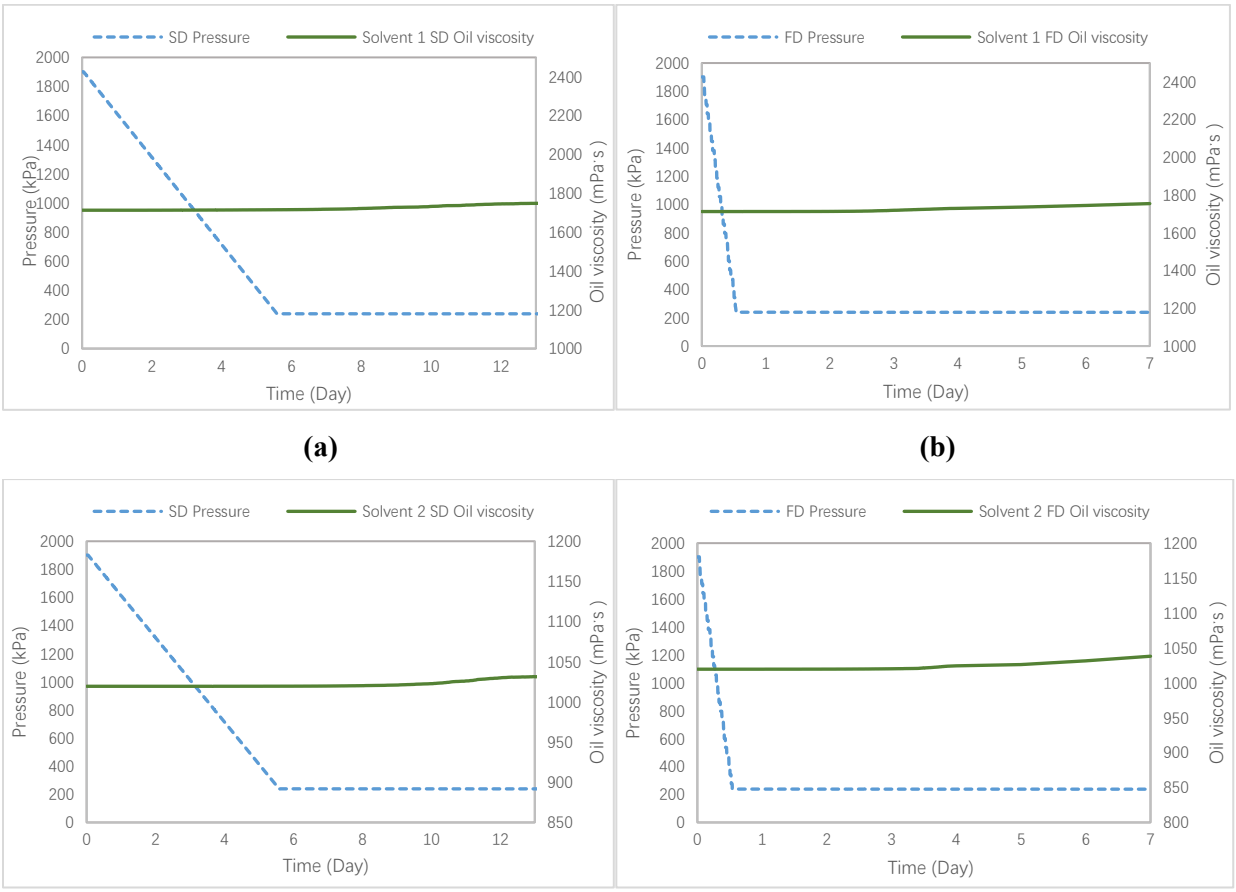

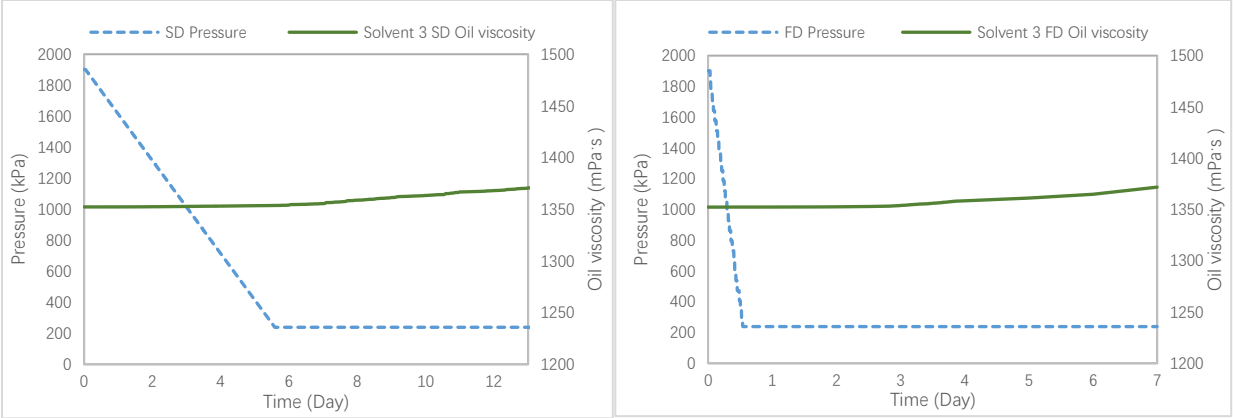

(e) **(f)**

Figure 4. 12: Simulated oil viscosity profiles for all three solvent systems under fast depletion (FD) and slow depletion (SD).

4.5 Effects of Solvent Compositions on Foamy Oil Behavior and Oil Production

Using the same fluid model as described in section 3, different combinations of C_3H_8-based and CO_2-based solvent mixtures, as summarized in **Table 4.4** and **Table 4.5**, are tested next. Each live oil system consists of 0.7 mole fraction of the primary component (dead oil), while the mole fraction of the solvent mixture is 0.3. The initial live oil viscosities corresponding to these two solvent systems are shown in the **Figure 4.10**. As expected, the oil viscosity decreases with increasing molar concentrations of CO_2 and C_3H_8, confirming that both CO_2 and C_3H_8 can effectively reduce the oil viscosity when dissolved in the heavy oil.

Table 4. 4: Description of the C_3H_8-based solvent compositions.

C_3H_8 Molar Concentration, %	100 (Pure)	80	50	35	10	0
CH_4 Molar Concentration, %	0	20	50	65	90	100 (pure)
Saturation Pressure (kPa)	1621	1983	2357	2948	4280	4809

Table 4. 5: Description of the CO_2-based solvent compositions.

CO_2 Molar Concentration, %	100 (Pure)	80	50	35	10	0
CH_4 Molar Concentration, %	0	20	50	65	90	100 (pure)
Saturation Pressure (kPa)	1929	2367	2896	3319	4430	4809

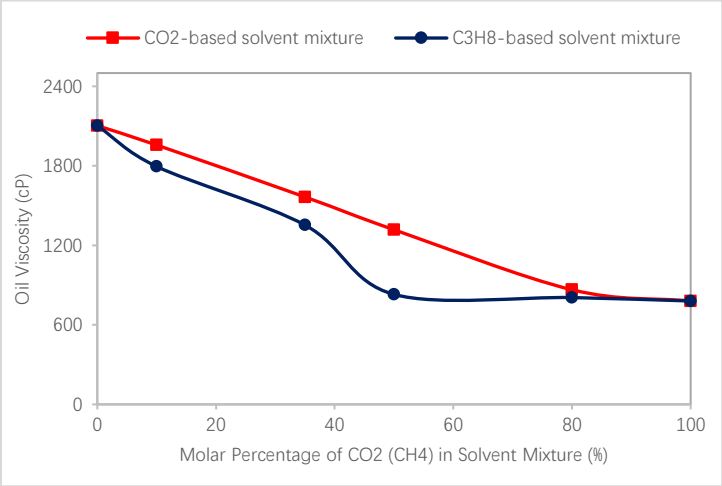

Figure 4. 13: Initial oil viscosity as a function of C_3H_8 or CO_2 molar concentration within the solvent mixture. Each system consists of 0.7 mole fraction of dead oil mixed with 0.3 mole fraction of solvent mixture.

Figures 4.14 to 4.16 compare the oil recovery performance of different C_3H_8-based and CO_2-based solvents, as well as those of the pure C_3H_8, CO_2 and CH_4 systems under both fast and slow depletion conditions. In the case of C_3H_8-based solvents, it has been established in the previous section that, due to the high solubility of C_3H_8, much fewer bubbles are formed. At moderate concentrations (i.e., 10%, 35%, 50% C_3H_8), the oil viscosity is reduced to C_3H_8 dissolution, and the oil recovery is slightly better than the pure CH_4. However, at much higher concentrations (i.e., >80% C_3H_8), the oil recovery is actually reduced; there is little foamy oil flow when the CH_4 concentration is so low. These results are in accordance with many previous observations: Bjorndalen et al. (2012) reported an absence of gas bubbles in the cell during their C_3H_8

experiments; Soh and Babadagli (2017) showed that C_3H_8 exhibited good mixing behavior with the heavy oil; however, the mixture of C_3H_8 and CH_4 displayed lower foaminess than pure CH_4, resulting in lower overall oil production. This result clearly shows the significance of the foamy oil mechanism on CSI performance: when there are few gas bubbles expanding and providing a driving energy for production, oil viscosity reduction alone due to solvent solubility will not be sufficient to induce incremental oil recovery. The ability of the solvent to partially leave solution is critical to CSI recovery. When a moderate amount of C_3H_8 is added (<50%), there is a slight improvement in the oil recovery factor, in comparison to the pure CH_4 case, especially after the pressure has declined to 200 kPag and all the CH_4 has evolved. This observation would further suggest that for the scale and time frame involved in this study, foamy oil flow is the main contributor to oil production, while viscosity reduction due to solvent in solution is less important. In contrast, CO_2-based solvents may yield higher oil recovery than pure CH_4 and C_3H_8 cases. The results in **Figure 4.15** show that higher compositions of CO_2 are beneficial for improving oil recovery. As explained in the previous sections, CO_2 has a higher solubility than CH_4 alone, so more gas is present in the oil and oil viscosity is reduced (similar to C_3H_8), but as the pressure drops, CO_2 is able to leave solution and generate more bubbles than C_3H_8. **Figure 4.16** also demonstrates that highest oil recovery is attained when pure CO_2 is used under both fast and slow pressure depletion conditions.

The results of these sand pack simulations offer important insights regarding the foamy oil flow characteristics and their impacts on oil recovery. First, fast depletion is often preferred for CHOPS operations to promote foamy oil flow, and the simulation results seem to suggest that fast depletion should also recommended for post-CHOPS CSI operations for the same reason. Second, although C_3H_8 is more soluble in the liquid phase and is able to reduce the oil viscosity, the lack of foaminess

within the time frame of flow represented in this study, renders this to be less effective, in comparison to CO_2, for improving oil flow rate. In other words, the ability to generate foamy oil flow within the time frame of flow is crucial. In the end, it is the interplay between viscosity reduction due to solvent dissolution and non-equilibrium gas exsolution that controls the production performance. Future studies should extend the modeling effort to assess the extent of C_3H_8-induced foamy oil flow at the field level, where the physical and time scales would be drastically different from the sand pack experiments.

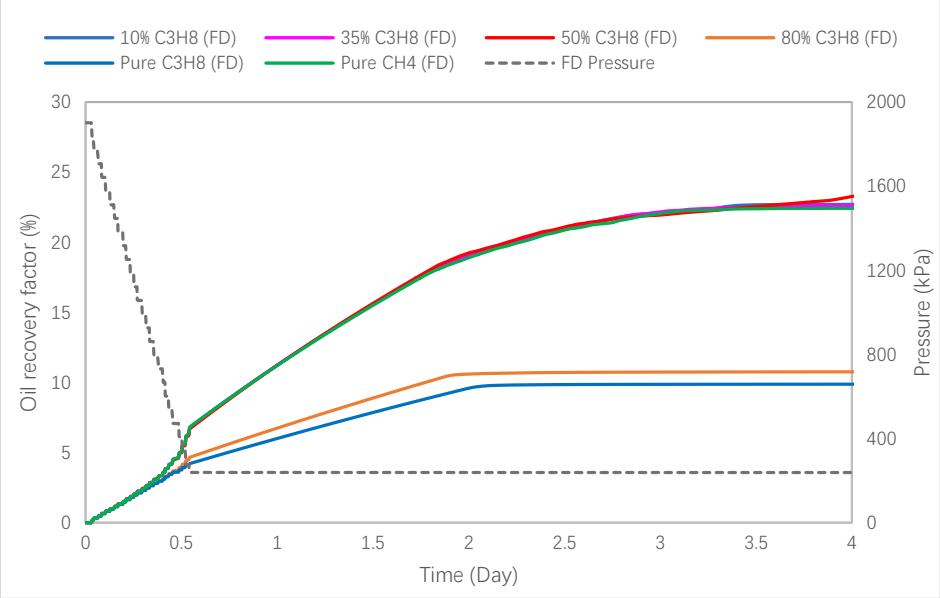

(a)

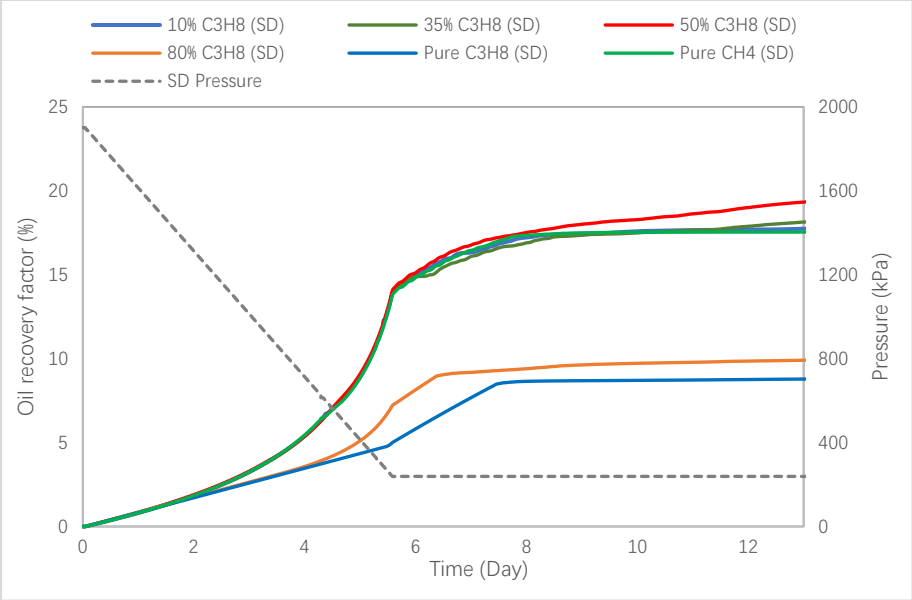

(b)

Figure 4. 14 Oil recovery comparison of C_3H_8-based solvents with different compositions: (a) fast depletion; (b) slow depletion.

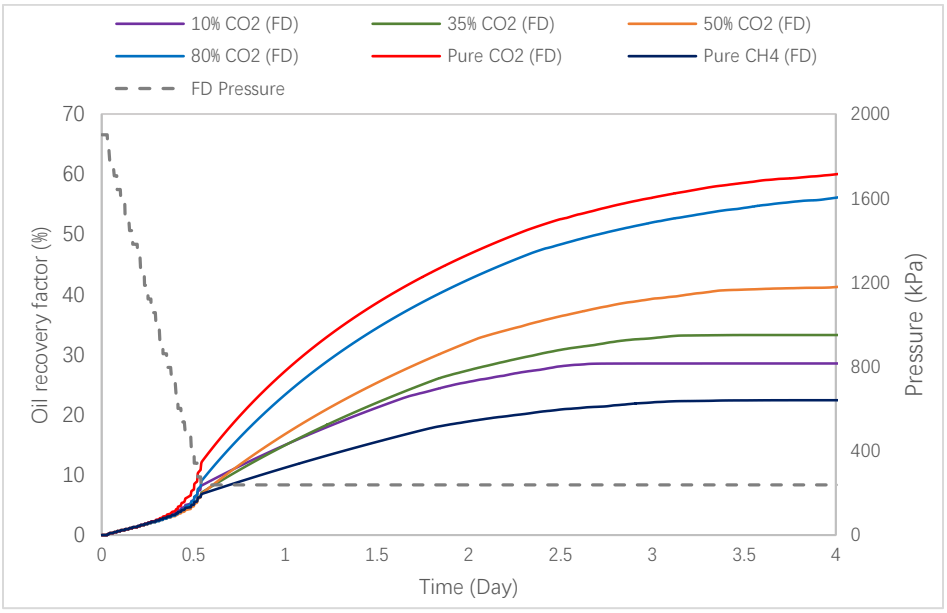

(a)

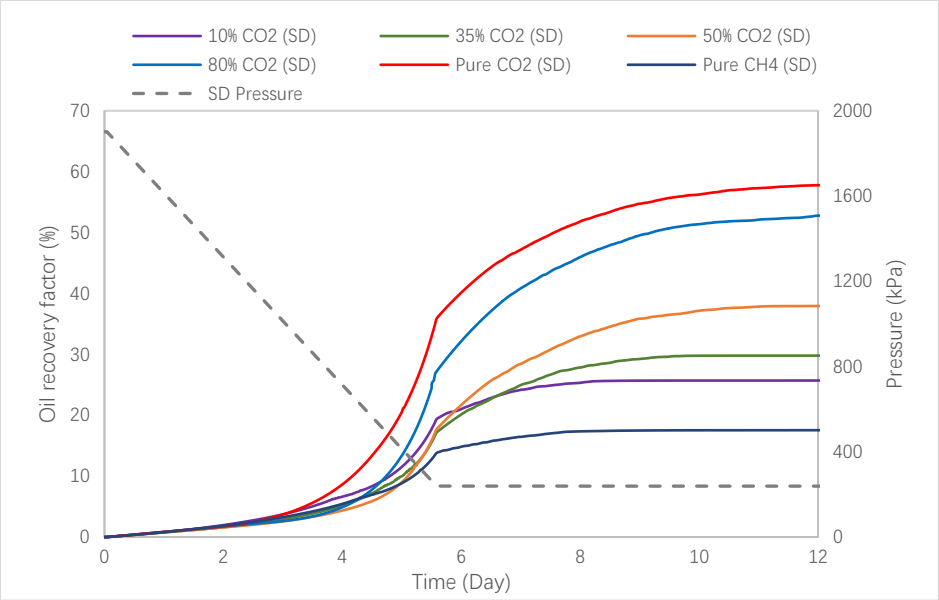

(b)

Figure 4. 15 Oil recovery comparison of CO_2-based solvents with different compositions: (a) fast depletion; (b) slow depletion.

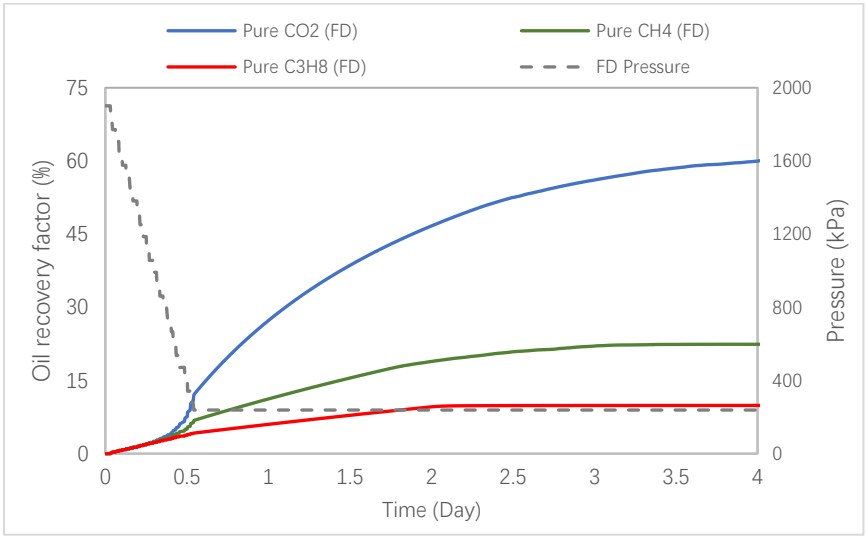

(a)

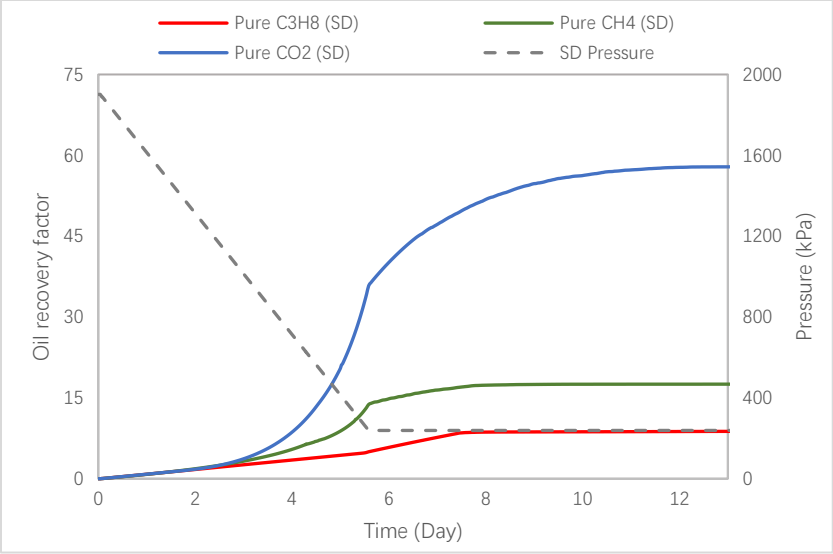

(b)

Figure 4. 16 Oil recovery comparison between pure C_3H_8, CO_2 and CH_4 solvents: (a) fast depletion; (b) slow depletion.

Chapter 5. Numerical Simulation in Post-CHOPS Reservoir

5.1 Overview

In this chapter, a field scale post-CHOPS model is constructed and upscaled from a core model, which was calibrated against detailed experimental data involving various propane-based (C_3H_8) and carbon dioxide-based (CO_2) solvent mixtures to analyze the impacts of simulation scales, heterogeneous wormholes, and the operating schedules on foamy oil behavior of different solvent systems. Reaction kinetics are implemented to represent the non-equilibrium gas dissolution and exsolution for foamy oil flow. A fractal wormhole network is modeled. To analyze the impacts of pressure depletion strategies, single stage pressure depletion involving three live oil-solvent systems, as well as two cycles of CSI production processes, are examined. Detailed sensitivity analyses involving different solvent compositions are discussed.

5.2 Reservoir Model Description

A 3D simulation model is constructed (CMG STARS User's Guide, 2016). The domain is discretized with a Cartesian mesh of 24 × 24 × 3 grid blocks along the x-, y-, and z-directions, with Δx = 1.25m; Δy = 1.25m; Δz = 0.375, 0.25, 0.375m. The physical dimensions of this model is 30 m × 30 m × 1 m. The model specifications are modified from a previous study by Martinez Gamboa and Leung (2019).

It is assumed that the wormholes are fully developed in the middle layer of the production formation, and the diffusion-limited aggregation (DLA) algorithm is used to generate the fractal

pattern of wormhole network. The DLA method was first introduced by Witten and Sander, 1981; Feder, 1988), then Liu and Zhao (2005) implemented a DLA algorithm to model the fractal patterns and they provided a convenient mathematical framework for capturing relevant characteristics. The fractal pattern grows around the wellbore, which is the geometrical center of the model. The sizes of the wormhole branches are closely to typical experimental and field observations, for instance, the wormhole diameter should gradually decrease from the wellbore to the tip of each brand (Martinez Gamboa and Leung, 2017). Multiple random realizations of 2D wormhole networks (30m × 30m) are generated, and all these wormhole networks have similar overall areal coverage, which is approximately 12% of the entire layer. Therefore, here one realization was picked as displayed in Figure 5.1. Porosity and permeability for the matrix as assigned based on averages of several CHOPS reservoirs in Saskatchewan. High porosity and permeability values are assigned to the wormhole grid blocks (Martinez Gamboa and Leung, 2017). The injector and producer are placed in center of the middle layer, as shown in **Figure 5.2**. Full description of the relevant reservoir properties of the numerical model are summarized in **Table 5.1** Water-oil and gas-liquid relative permeability relationships are shown in **Figure 4.3**.

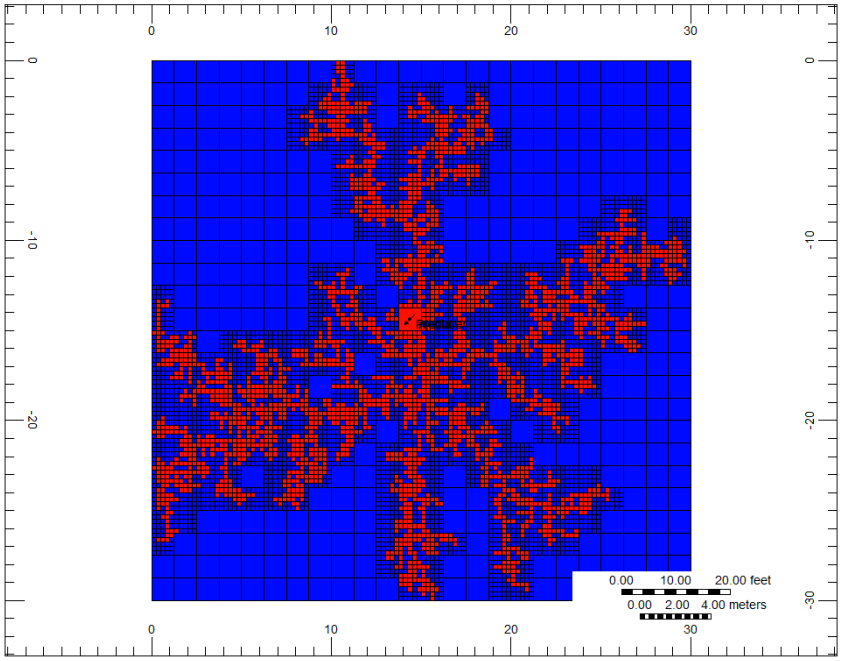

Figure 5. 1 Wormholes fractal pattern in the middle layer.

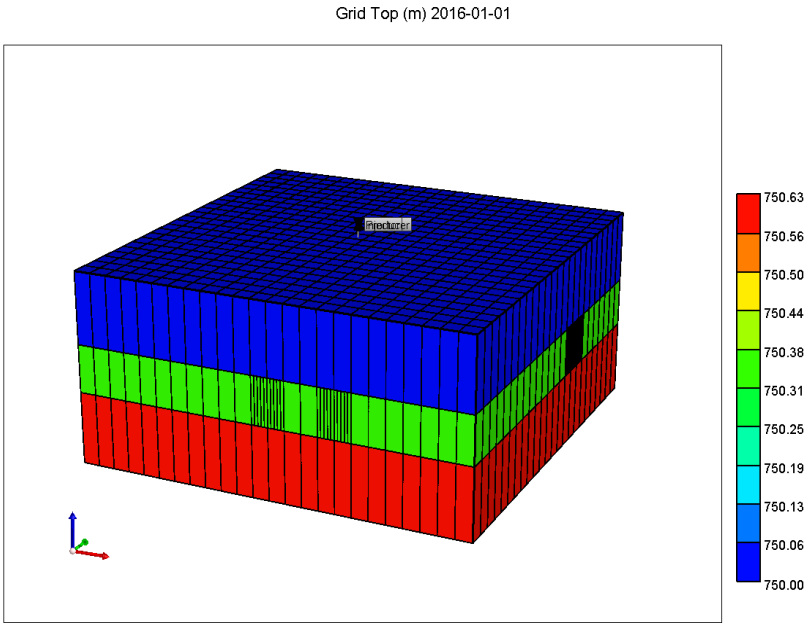

Figure 5. 2: 3-D view of the reservoir model.

Table 5. 1: Reservoir properties of the field model.

Parameters	value
Depth (m)	750
Reservoir Pressure (kPa)	4000
Reservoir Temperature (℃)	20
Bottom-hole Pressure BHP (kPa)	500
Wormhole Porosity (fraction)	0.60
Matrix Porosity (fraction)	0.30
Wormhole permeability (Darcy)	60
Matrix permeability (Darcy)	3
Rock compressibility (Pa^{-1})	3×10^{-6}
Diffusion Coefficient (cm^2/s)	0.001

5.3 Results and Discussion

5.3.1 Single-Stage Pressure Depletion Tests

In this set of simulations, the field-scale model is depleted from an initial condition of 4000 kPa and 20 ºC to the minimum bottom-hole pressure of 500 kPa. Given the in-situ fluid is at its live oil saturated condition, this single stage of depletion could be regarded as the production stage of one CSI cycle. A depletion rate of 50 kPa/day is employed (Martinez Gamboa and Leung, 2017). A total production time of 150 days is simulated (Martinez Gamboa and Leung, 2017; Dusseault, 2007). For the pressure depletion processes, the kinetic model, as described by **Eqs. (4-18 to 4-23)**, is used to model the foamy oil mechanics.

5.3.1.1 Oil Recovery Performance

As discussed earlier, three solvent mixtures were used in the lab experiments, and the same compositions are used in the simulation models. Solvent 1 (35% CO_2 and 65% CH_4) and Solvent 2 (80% CO_2 and 20% CH_4) are CO_2-based solvent mixtures and Solvent 3 (35% C_3H_8 and 65% CH_4) is a propane-based solvent mixture. The oil production profiles corresponding to these heavy oil-solvent systems during the pressure depletion stage are shown in **Figure 5.3**. For the CO_2-based solvent systems, Solvent 2 with higher CO_2 content produces more oil than Solvent 1; the results are reasonable, as CO_2 is the primary solvent, and the higher its molar concentration, the higher the oil recovery factor would be. Solvent 3 shows a similar oil production behavior as Solvent 2. However, there is only 35% C_3H_8 in Solvent 3, as opposed to 80% CO_2 in Solvent 2; the results in **Figure 5.3** would imply that C_3H_8 is a more effective solvent at the field scale. This conclusion differs from the results reported in previous study involving core-scale depletion models. It was clear that for the lab-scale experiment, C_3H_8 did not have the opportunity to leave solution and form the foamy oil. The results from that study demonstrated the significance of the foamy oil mechanism on CSI performance: when there are few gas bubbles expanding, oil viscosity reduction alone due to solvent solubility would be insufficient to contribute to the overall oil recovery. It is crucial that the solvent would partially leave solution. It was concluded that for the scale and time frame involved in that study, foamy oil flow was the main contributor to oil production, while viscosity reduction due to solvent in solution was less important.

There are a few explanations for that observation: (1) the time duration is too short (< 2 weeks) and the model size is limited (approximately 11 cm in length); (2) the high solubility of C_3H_8 renders it to be less effective for generating foamy oil flow. The core-scale simulation results seem

to suggest that CO_2-based solvents (i.e., Solvent 1 and Solvent 2) are more effective: more foamy oil flow and higher oil recovery. Therefore, the field-scale simulation results presented here are consistent with the previous finding, in the sense that the increase in time and length scales associated with the field-scale model has facilitated an increased release of C_3H_8, such that higher oil production is observed for Solvent 3 due to an increase in foaminess.

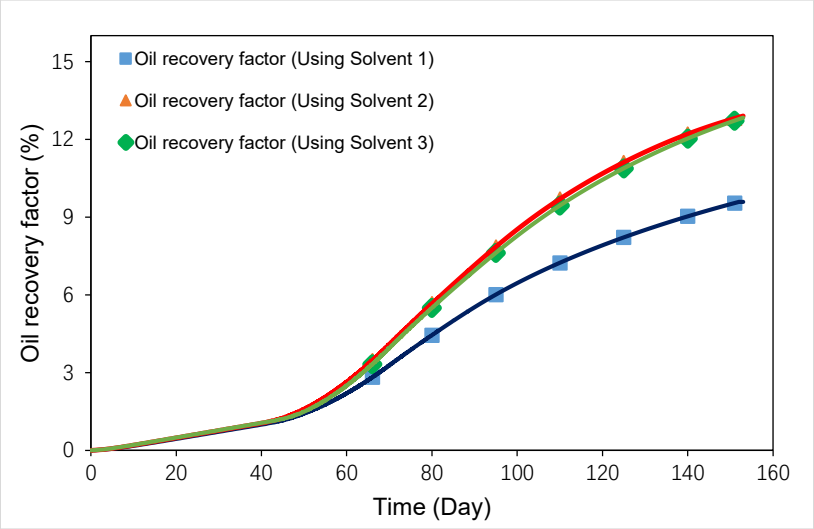

Figure 5. 3: Oil recovery factor profiles corresponding to the three heavy oil-solvent systems.

5.3.1.2 Foamy Oil Flow and Dispersed Bubble Gas Behavior

The dispersed gas bubbles in the liquid phase are the main characteristics of foamy oil flow, which has a positive effect on oil production: (1) the gas flow rate is reduced due to a decrease in free gas saturation and (2) oil viscosity is decreased. **Figure 5.4** compares the bubble gas mole fraction in oleic (liquid) phase corresponding to the three solvent systems under fast (100kPa/day) and slow (base case, 50kPa/day) conditions. It illustrates that faster pressure depletion rate leads to more dispersed gas bubbles for all three live oil-solvent systems. The amount of dispersed bubbles is the largest for Solvent 1 with lower concentration of CO_2 generates the largest amount of dispersed

bubbles among three live oil-solvent systems; however, the corresponding oil production and viscosity reduction are also the lowest. Although more oil is recovered for the Solvent 3 system, in comparison to the other two solvents, the associated total amount of gas bubbles is the lowest; this observation would suggest that the extent of foamy oil flow (i.e., amount of gas bubbles in the liquid phase) is not the only controlling factor for oil recovery.

Solvent solubility, however, remains a key factor that influences the oil recovery, particularly in the field-scale simulation. C_3H_8 with higher solubility in the heavy oil tends to be more effective than CO_2: Solvent 2 with higher CO_2 concentration produces exhibits similar oil recovery performance as Solvent 3. As discussed earlier, foamy oil flow behavior of C_3H_8 is quite sensitive to the physical scale and time duration, as limited solvent release and foamy oil flow was observed for C_3H_8 at the lab-scale settings.

Figure 5.5 examines the spatial distribution of gas bubbles for CO_2-based solvent (Solvent 2) and C_3H_8-based (Solvent 3) systems after 75 days; it is clear that more bubbles are located in the near-well region; a plausible explanation is that the drastic pressure drop near the well has offered a favorable condition for gas bubble formation. It is also noted that there are fewer C_3H_8 bubbles (Figure 5.5a) than CO_2 gas bubbles (Figure 5.5b). The CO_2 dispersed bubbles also exist at a distance farther away from the wellbore, in comparison to the C_3H_8 bubbles. This phenomenon illustrates that there is more CO_2 release from the liquid, and this trend is also observed from the core-scale simulation results. The amount of dispersed bubbles is also affected by the wormhole heterogeneity; for instance, the higher wormhole intensity near the wellbore region results in larger fluxes and more significant pressure drop; these conditions would favor the gas exsolution and generation of more dispersed bubbles in the near-well region.

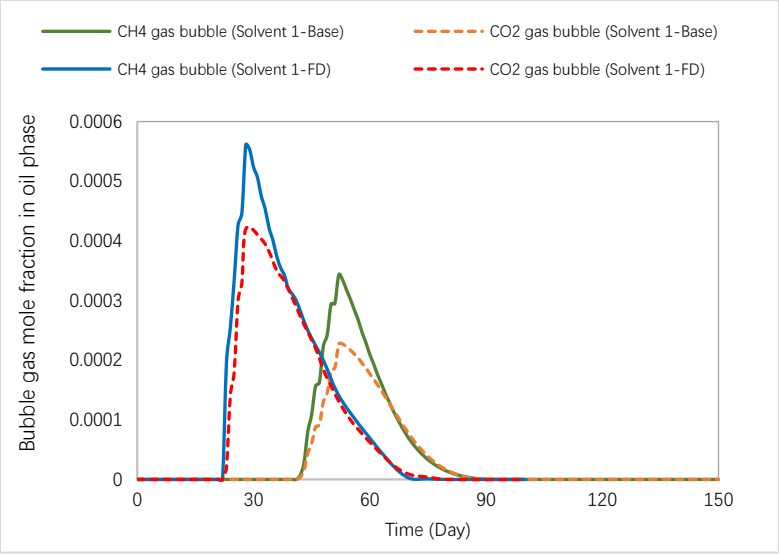
CH4 gas bubble (Solvent 1-Base)
CO2 gas bubble (Solvent 1-Base)
CH4 gas bubble (Solvent 1-FD)
CO2 gas bubble (Solvent 1-FD)
Bubble gas mole fraction in oil phase
0.0006
0.0005
0.0004
0.0003
0.0002
0.0001
0
0
30
60
90
120
150
Time (Day)

(a)

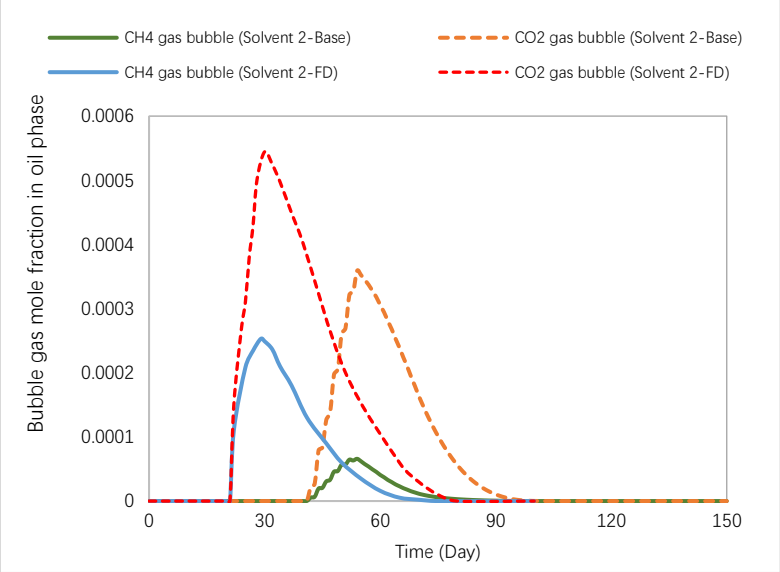
CH4 gas bubble (Solvent 2-Base)
CO2 gas bubble (Solvent 2-Base)
CH4 gas bubble (Solvent 2-FD)
CO2 gas bubble (Solvent 2-FD)
Bubble gas mole fraction in oil phase
0.0006
0.0005
0.0004
0.0003
0.0002
0.0001
0
0
30
60
90
120
150
Time (Day)

(b)

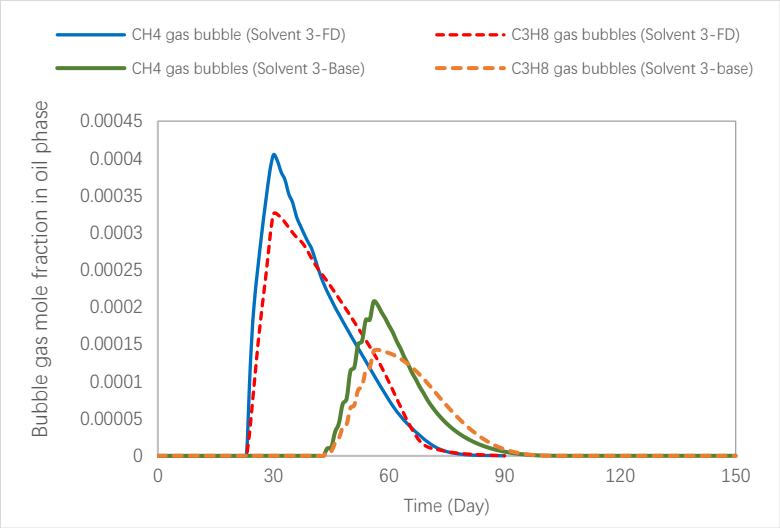

(c)

Figure 5. 4: Comparisons of bubble gas mole fraction in the liquid phase under fast and base (slow) conditions at the producer for the field-scale pressure depletion simulation: (a) Heavy oil-Solvent 1 system; (b) Heavy oil-Solvent 2 system; (c) Heavy oil-Solvent 3 system.

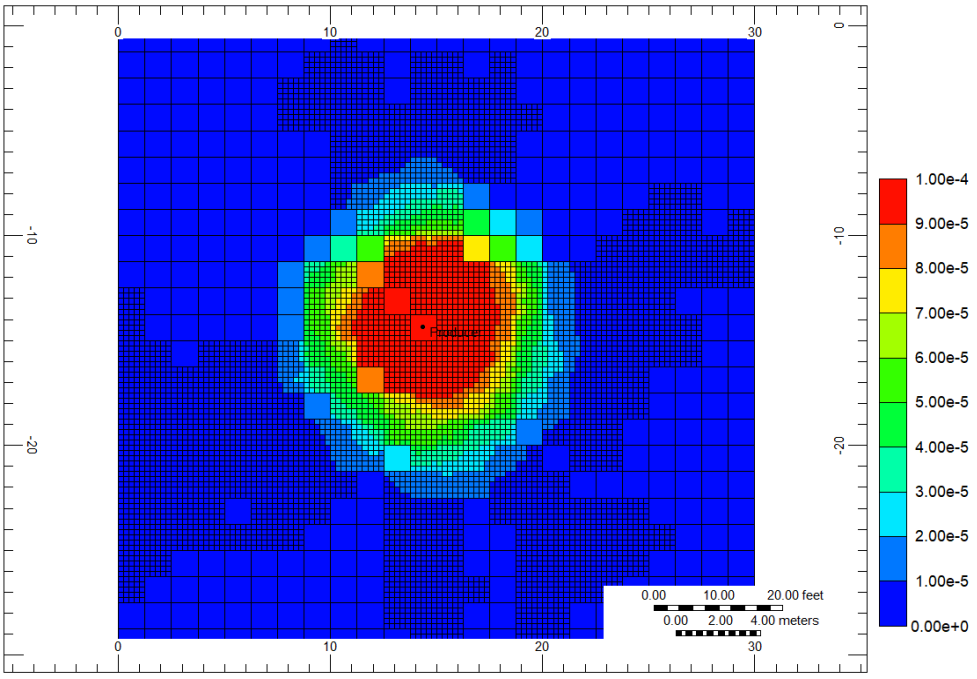

(a)

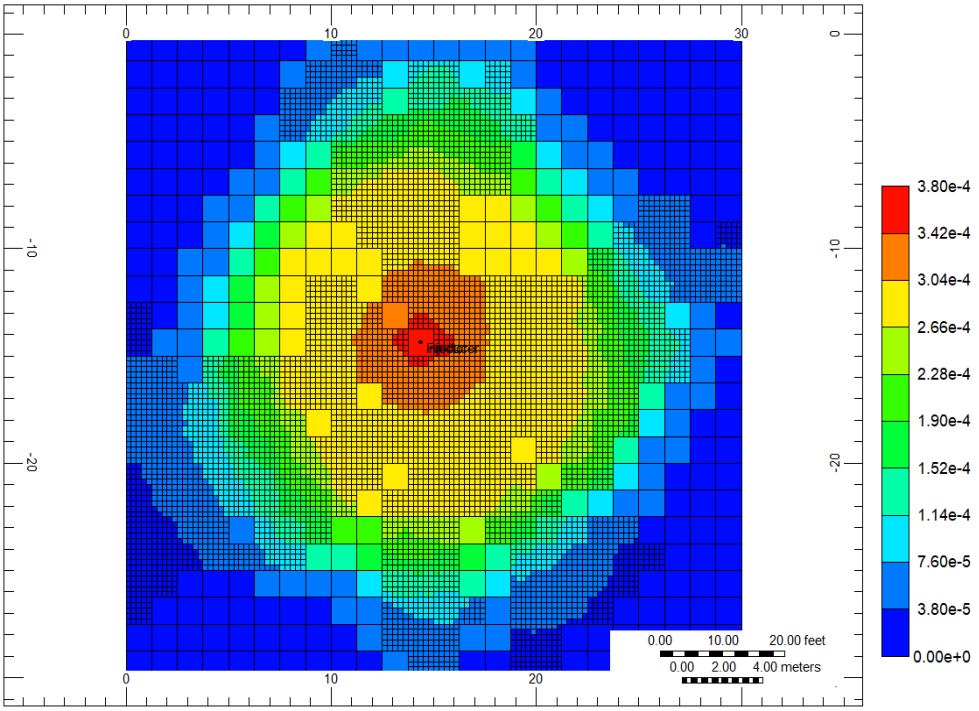

(b)

Figure 5. 5: Spatial distribution after 75 days of pressure depletion: (a) C_3H_8 bubbles for the heavy oil-Solvent 3 system; (b) CO_2 bubbles for the heavy oil-Solvent 2 system.

5.3.1.3 Foamy Oil Viscosity

The liquid viscosity profiles corresponding to the three solvent systems are presented in **Figure 5.6**, and the initial live oil viscosities are also presented in **Table 5.2**. During the pressure depletion process, the viscosity has increased slightly for all three solvent systems, indicating that both solvent solubility and non-equilibrium solvent release is beneficial for reducing the liquid viscosity. As discussed earlier, **Figure 5.3** shows that both Solvents 2 and 3 have yielded comparable oil recovery, which is much higher than that for Solvent 1. This is because the oil (liquid) viscosities for Solvent 2 and Solvent 3 are much lower than that for Solvent 1.

Several conclusions can be drawn from the discussions in **sections 5.3.1.1** to **5.3.1.3**. Firstly, for the field case reservoir model, the total amount of dispersed bubbles may not be the only driver

for viscosity reduction and oil production. The largest amount of dispersed bubbles is observed for Solvent 1 (**Figure 5.4**); however, the corresponding oil production and viscosity reduction are the lowest. Secondly, more foamy oil flow is achieved using C_3H_8 at the field scale than what is noted from the core-scale models. From **Figure 5.5**, the spatial area of CO_2 bubbles for Solvent 2 system is distributed wider than C_3H_8 bubbles for Solvent 3 system, and it might be concluded that both CO_2-based Solvent 2 and C_3H_8-based Solvent 3 are good choice for heavy oi production, since for Solvent 2, there are more dispersed gas bubbles distributed in the area, even though there is lower solubility of CO_2 than C_3H_8; for Solvent 3, although the amount of gas bubbles are not much at the place away from the well, the high solubility contributes to high oil recovery.

The simulation results of this study would suggest that propane-based solvents may outperform CO_2-based solvents on a mole-by-mole basis. However, the results also suggest that similar level of viscosity reduction and oil production can be achieved with solvents with high CO_2 content, due to the enhanced foamy oil flow behavior associated with CO_2. Considering the costs of CO_2 disposal, as well as the costs of C_3H_8 extraction, the utilization of CO_2-based solvents may offer economic benefits.

Table 5. 2: Initial fluid viscosities corresponding to three heavy oil-solvent systems.

Heavy oil-Solvent system	Initial viscosity (mPa·s)
Heavy oil-Solvent 1	2878.8
Heavy oil-Solvent 2	2118.9
Heavy oil-Solvent 3	1856.5

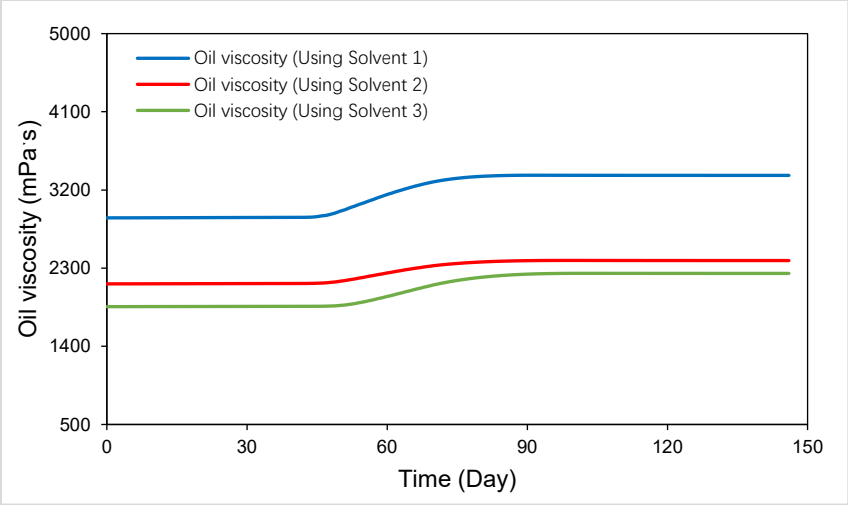

Figure 5. 6: Oil viscosity corresponding to three heavy oil-solvent systems.

5.3.1.4 Effect of Pressure Depletion Rate

The oil recovery comparison between fast and slow pressure depletion conditions are shown in Figure 5.7. For all three solvent systems, higher pressure depletion rate leads to higher oil production, which is consistent with the core-scale simulation results and other previous studies (Smith, 1986; Maini et al, 1993; Soh et al., 2017).

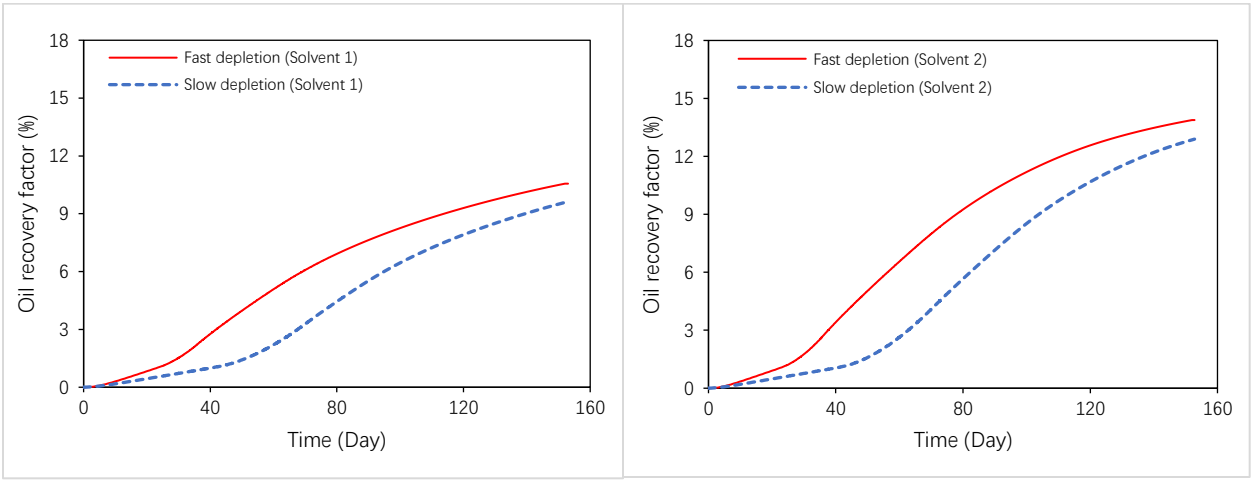

(a) **(b)**

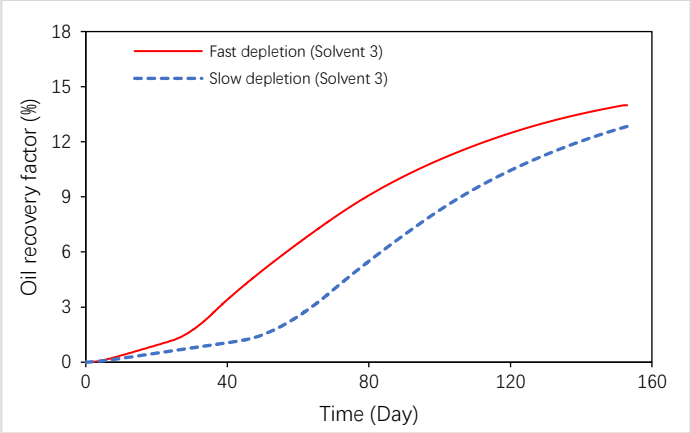

(c)

Figure 5. 7: Oil recovery profiles for fast and slow depletion rate: (a) Heavy oil-Solvent 1 system; (b) Heavy oil-Solvent 2 system; (c) Heavy oil-Solvent 3 system.

Several conclusions can be drawn from the discussions in sections 3 thus far. Firstly, for the field case reservoir model, the total amount of dispersed bubbles may not be the only driver for viscosity reduction and oil production. The solubility of different solvent systems seems to be a more important factor for heavy oil production in field scale simulation. The simulation results of this study would suggest that propane-based solvents may outperform CO_2-based solvents on a mole-by-mole basis. The high solubility of C_3H_8 contributes to the high oil recovery associated with C_3H_8-based solvents at the field scale. However, the results also suggest that similar level of viscosity reduction and oil production can be achieved with solvents with high CO_2 content, due to the enhanced foamy oil flow behavior associated with CO_2. Considering the costs of CO_2 disposal, as well as the costs of C_3H_8 extraction, the utilization of CO_2-based solvents may offer economic benefits.

5.3.2 Post-CHOPS CSI Processes – Simulation of Non-Equilibrium Solvent Dissolution and Exsolution

In this section, the initial pressure depletion stage is followed by a full cycle of injection (30 days), soaking (15 days), and production (150 days). The AITF kinetic model, as described by **Eqs. (4-15 to 4-23)**, is used to model the foamy oil mechanics. The surface gas injection rate is set at 150 m^3/day, such that the reservoir can be re-pressurized close to its initial pressure by the end of the injection period, such that the solvent solubility would be high and the reservoir becomes re-energized for production (Chang et al., 2013). The pressure depletion rate (50 kPa/day) is same as the base case.

5.3.2.1 Oil Recovery Performance and Foamy Oil Viscosity

Profiles of oil recovery, liquid viscosity and pressure variation corresponding to the three solvent systems are compared in **Figure 5.8**. Similar to the observations obtained from the single stage pressure depletion tests (section 3.1), both Solvents 2 and 3 have yielded comparable oil recovery, which is much higher than that for Solvent 1, as the oil (liquid) viscosities for Solvent 2 and Solvent 3 are much lower than that for Solvent 1.

The oil (liquid) viscosity profiles in **Figure 5.8 (b)** confirm that the viscosity would increase with pressure decline and decrease as more solvent is injected into the reservoir. Moreover, the viscosity increases gradually after the pressure has decline due to the presence of dispersed gas bubbles.

The bottom-hole pressure schedules are shown in **Figure 5.8 (c)**. The results illustrate that during the injection period, the bottom-hole pressure corresponding to Solvent 1 system increases more rapidly to a higher level than the other two solvent mixtures. This is because Solvent 1 is less soluble in the heavy oil (also with lower diffusion rate), a relatively rapid rise in the injection

pressure would be expected (Ivory et al., 2010). Comparing between Solvents 1 and 2, Solvent 2 has higher molar concentration of CO_2; therefore, solubility for Solvent 2 is higher; comparing between Solvents 1 and 3, solubility for Solvent 3 is higher because of its C_3H_8 content.

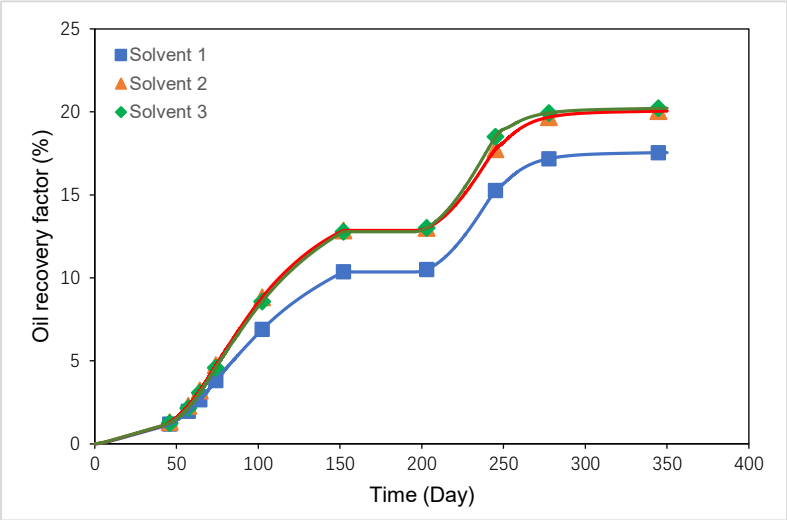

(a)

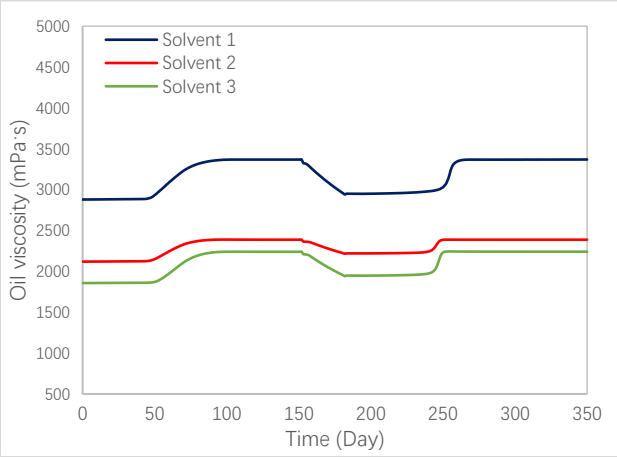

(b)

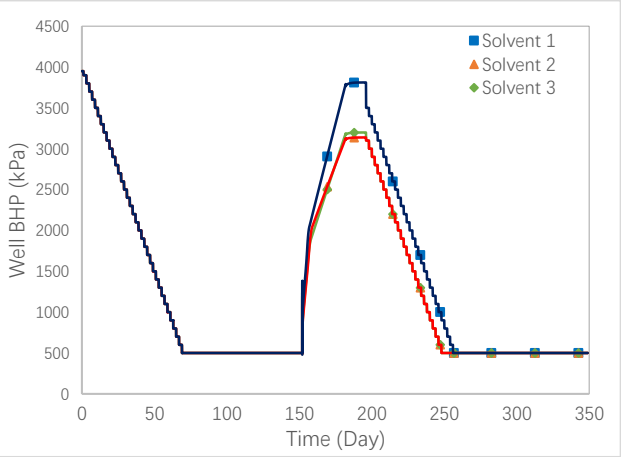

(c)

Figure 5. 8: Simulation results of the CSI model (pressure depletion + one full cycle) for all three live oil-solvent systems (a) Oil recovery factor; (b) oil (liquid) viscosity profiles; (c) well bottom-hole pressure.

5.3.2.2 Comparison with an alternative gas exsolution kinetic model

Previously, the gas exsolution process is described according to Eqs. 4-18 to 4-23, where a two-step process is used to describe the liberation of dissolved gas to trapped gas and the coalescence of dispersed gas bubbles to a continuous gas phase. In this section, a different kinetic model, as described in **Eqs. 5-1** to **5-3**, is compared, where the entire gas exsolution process is represented in a single reaction (Ivory *et al.,* 2010) The non-equilibrium gas dissolution processes for the post-CHOPS CSI process remain unchanged, as described in Eqs. 4-15 to 4-17.

$$CH_4\ (L) \rightarrow CH_4\ (G) \tag{5-1}$$

$$C_3H_8\ (L) \rightarrow C_3H_8\ (G) \tag{5-2}$$

$$CO_2\ (L) \rightarrow CO_2\ (G) \tag{5-3}$$

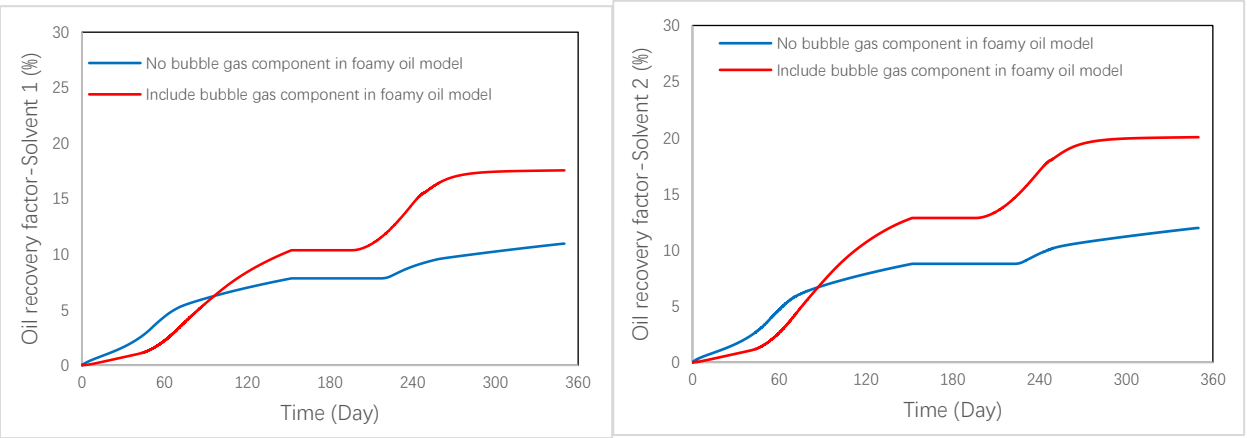

(a) **(b)**

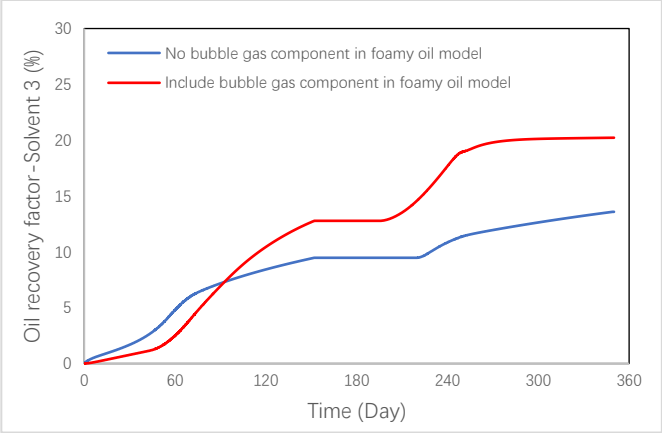

(c)

Figure 5. 9: Oil recovery profiles corresponding to the two different foamy oil modeling approaches adopted in the field-scale CSI simulation: (a) Live oil-Solvent 1 system; (b) live oil-Solvent 2 system; (c) live oil-Solvent 3 system.

Figure 5.9 compares the oil production corresponding to these two gas exsolution kinetic models. For all three solvent systems, higher oil production is observed for the two-step kinetic model. There is an added computational cost associated with the two-step approach, especially for field-scale model (approximately twice as long as the simpler single-step approach); however, incorporating the proper non-equilibrium foamy oil physics seem to justify this additional computational requirement.

The limitations of this field scale simulation are that as lack of both detailed experimental data and field production data, same kinetic reaction constants as the history-matched Solvent 3 are used for all cases; for the gas dissolution processes in post-CHOPS simulation, the assumed kinetic rate was adopted. Further study should capture more detailed laboratory and field data using more valid kinetic reaction constants to better analyze the foamy oil behaviors in different simulation scales.

Chapter 6. Conclusions and Recommendations

6.1 Conclusions

In this study, a mechanistic simulation model is constructed and calibrated against experimental measurements from a series of pressure depletion tests. A fluid model is defined based on equilibrium saturation pressures and gas-oil ratios corresponding to different combinations of solvent and dead oil. A viscosity model is formulated using measurements at different temperatures and solvent-oil mixtures. Reaction kinetics is implemented to represent the non-equilibrium exsolution of gas from solution gas to bubble gas and free gas in foamy oil flow. The field model is upscaled from the core model to analyze the impacts of simulation scales, heterogeneous wormholes, and the operating schedules on foamy oil behavior of different solvent systems.

(1) The results of these sand pack simulations offer important insights regarding the foamy oil flow characteristics and their impacts on oil recovery. Both C_3H_8-based and CO_2-based solvents exhibit foamy oil behavior under fast and slow pressure depletion rates. The oil viscosity remains close to the initial live oil viscosity throughout the pressure depletion process.

(2) By comparing the oil production of Solvent 1 (35% CO_2) and Solvent 2 (80% CO_2), the results show that higher molar percentage of CO_2 is beneficial for improving oil recovery. More gas bubbles are formed in Solvent 2 system, which is the reason for higher oil recovery. This observation is also consistent with field-scale simulation results.

(3) The core-scale simulation results demonstrate that although C_3H_8 is more soluble in the liquid phase and it reduces oil viscosity to a lower value, the lack of foaminess renders this to be less effective, in comparison to CO_2 for improving oil flow rate. In addition, foamy oil flow is more stable and dominant when CO_2, instead of C_3H_8, is used: more gas bubbles are formed and remain in the oil phase. Therefore, in core-scale simulation study, CO_2 is observed to be the optimal solvent with higher oil production than C_3H_8.

(4) Both core-scale and field-scale simulation results show that fast depletion is beneficial for higher oil recovery, as is generally preferred for CHOPS operations.

(5) For the field-scale post-CHOPS simulation study, a detailed up-scaled simulation model is constructed. C_3H_8 is more sensitive to the changes of physical scale and time duration from core to field-scale models than CO_2 in terms of foamy oil behavior and oil production. The higher intensity of wormholes near the wellbore region results in larger fluxes, more significant pressure dropping and generation of more dispersed bubbles. This developed field-scale simulation model is useful for providing important insights regarding the interplay between wormhole heterogeneity, time scale and non-equilibrium solvent dis(ex)solution on the characteristics of foamy oil flow and oil recovery at the field level.

(6) From the results of field-scale simulation, considering the advantages and disadvantages for the two solvents: C_3H_8 and CO_2, it can be concluded that C_3H_8 is the more soluble, while CO_2 can generate more dispersed bubbles (better foamy oil flow characteristics). The results demonstrate that the total amount of dispersed bubbles may not be the only driver for viscosity reduction and oil production. In the end, it is the interplay between the foaminess, solvent solubility, and time scale that controls the overall recovery performance. C_3H_8-based solvents seem to be more effective than CO_2-based solvents, at least on a mole-by-mole basis. However, the results would

also suggest solvents with high CO_2 content could achieve similar level of viscosity reduction and oil production as solvents of lower C_3H_8 content. The significance of this observation is that, considering the costs of CO_2 disposal, as well as the costs of C_3H_8 extraction, the utilization of CO_2-based solvents may offer several economic benefits.

(7) Results from the CSI simulation (pressure depletion + one full cycle) illustrate the significance of solvent solubility in foamy oil flow, liquid viscosity reduction, and oil production enhancement. In addition, less rapid increase in the bottom-hole pressure is observed when the solvent is more soluble with the heavy oil.

6.2 Future work

(1) Currently there are inconsistences regarding the solvent (e.g., C_3H_8, CO_2 and CH_4) foamy oil behavior in both experimental and numerical simulation study. More detailed and valid data from laboratory experiments and field pilots are required for further study on non-equilibrium gas dissolution/exsolution processes of foamy oil flow.

(2) This simulation study is on the basis of a set of experimental data, however, the gravity effects were not considered as a factor that impacts foamy oil behavior during pressure depletion processes. More than that, further study of using other solvent types and combinations in post-CHOPS are needed in both core and field scales.

(3) The scaled-up modeling in this study is conducted in a modified post-CHOPS reservoir model, since lack of real production data from pilot tests, same kinetic reaction constants as core-scale model are applied. Some results obtained from field model are consistent with sand pack observations, while some are not. To better understand solvents non-equilibrium foamy oil

behavior in field-scale reservoirs, realistic post-CHOPS CSI production data are required. Further study on the foamy oil behavior of C_3H_8 in different physical scales as well as different operating conditions should be investigated.

Bibliography

Alshmakhy, A., & Maini, B. B. (2012). Effects of gravity, foaminess, and pressure drawdown on primary-depletion recovery factor in heavy-oil systems. *Journal of Canadian Petroleum Technology*, *51*(06), 449-456.

Alvarez, J., Sawatzky, R. P., & Moreno, R. (2014, September). Heavy-Oil Waterflooding: Back to the Future. In SPE Heavy and Extra Heavy Oil Conference: Latin America. Society of Petroleum Engineers.

Arefmanesh, A., Advani, S. G., & Michaelides, E. E. (1992). An accurate numerical solution for mass diffusion-induced bubble growth in viscous liquids containing limited dissolved gas. *International Journal of Heat and Mass Transfer*, *35*(7), 1711-1722.

Arora, P., & Kovscek, A. R. (2001, January). Mechanistic Modeling of Solution Gas Drive in Viscous Oils. In SPE International Thermal Operations and Heavy Oil Symposium. Society of Petroleum Engineers.

Bera, A., & Babadagli, T. (2016). Relative permeability of foamy oil for different types of dissolved gases. *SPE Reservoir Evaluation & Engineering*, *19*(04), 604-619.

Bjorndalen, N., Jossy, E., & Alvarez, J. (2012). Foamy oil behaviour in solvent based production processes. SPE Paper 157905 presented at the SPE Heavy Oil Conference Canada, Calgary, Alberta, Canada, June 12-14.

Bora, R., Chakma, A., & Maini, B. B. (2003, January). Experimental investigation of foamy oil flow using a high pressure etched glass micromodel. In SPE Annual Technical Conference and Exhibition. Society of Petroleum Engineers.

Bryan, J., Butron, J., Nickel, E., & Kantzas, A. (2018). Measurement of Non-Equilibrium Solvent Release from Heavy Oil during Pressure Depletion. SPE Paper 189729 presented at the SPE Canada Heavy Oil Technical Conference, Calgary, Alberta, Canada, March 13-14.

Busahmin, B. S., & Maini, B. B. (2010, January). Effect of solution-gas-oil-ratio on performance of solution gas drive in foamy heavy oil systems. In *Canadian Unconventional Resources and International Petroleum Conference*. Society of Petroleum Engineers.

Butler, R. M., & Mokrys, I. J. (1991). A new process (VAPEX) for recovering heavy oils using hot water and hydrocarbon vapour. Journal of Canadian Petroleum Technology, 30(01).

Chang, J., & Ivory, J. (2013). Field-scale simulation of cyclic solvent injection (CSI). *Journal of Canadian Petroleum Technology*, *52*(04), 251-265.

Chang, J., & Ivory, J. (2015, June). History Match and Strategy Evaluation for CSI Pilot. In *SPE Canada Heavy Oil Technical Conference*. Society of Petroleum Engineers.

Claridge, E. L. (1995). A proposed model and mechanism for anomalous foamy heavy oil behavior. SPE Paper 29243 presented at the SPE International Heavy Oil Symposium, Calgary, Alberta, Canada, June 19-21.

CMG (2016). STARS User's Guide, Computer Modeling Group Ltd.

CMG (2016). WinProp User's Guide, Computer Modeling Group Ltd.

Coombe, D., & Maini, B. (1994, April). Modeling foamy oil flow. In Workshop on Foamy Oil Flow, Petroleum Recovery Institute, Calgary, AB, Canada, Apr (Vol. 27).

Coombe, D., Tremblay, B., Tran, D., & Ma, H. (2001, January). Coupled hydro-geomechanical modelling of the cold Production process. In *SPE International Thermal Operations and Heavy Oil Symposium*. Society of Petroleum Engineers.

Cuthiell, D., Kissel, G., Jackson, C., Frauenfeld, T., Fisher, D., & Rispler, K. (2006). Viscous fingering effects in solvent displacement of heavy oil. Journal of Canadian Petroleum Technology, 45(07).

David, N. A. (2018). *Experimental and Numerical Investigation of Cyclic Solvent Injection (CSI) Performance in Heavy Oil Systems In The Presence of Wormhole Networks* (Doctoral dissertation, Faculty of Graduate Studies and Research, University of Regina).

Du, C., & Yortsos, Y. C. (1999). A numerical study of the critical gas saturation in a porous medium. Transport in Porous Media, 35(2), 205-225.

Du, Z., Peng, X., & Zeng, F. (2018). Comparison analyses between the linear and non-linear pressure-decline methods in cyclic solvent injection (CSI) process for heavy oil recovery. Fuel, 224, 442-450.

Du, Z., Zeng, F., & Chan, C. (2014, June). Effects of pressure decline rate on the post-CHOPS cyclic solvent injection process. In *SPE Heavy Oil Conference-Canada*. Society of Petroleum Engineers.

Du, Z., Zeng, F., Peng, X., & Chan, C. (2018). Experimental and material balance equations analyses of cyclic solvent injection based on a large 3D physical model. Fuel, 215, 915-927.

Dumore, J. M. (1970). Development of gas-saturation during solution-gas drive in an oil layer below a gas cap. *Society of Petroleum Engineers Journal*, *10*(03), 211-218.

Dusseault, M. (1993). Cold production and. Enhanced oil recovery. Journal of Canadian Petroleum Technology, 32(09).

Dusseault, M. B. (2001, January). Comparing Venezuelan and Canadian heavy oil and tar sands. In Canadian international petroleum conference. Petroleum Society of Canada.

Dusseault, M. B., & El-Sayed, S. (1999, August). CHOP-Cold Heavy Oil Production. In *IOR 1999-10th European Symposium on Improved Oil Recovery*.

Egermann, P., Vizika, O., Dallet, L., Requin, C., & Sonier, F. (2000, January). Hysteresis in three-phase flow: experiments, modeling and reservoir simulations. In SPE European Petroleum Conference. Society of Petroleum Engineers.

Engineering ToolBox, (2004). Retrieved from https://www.engineeringtoolbox.com/pressure-d_587.

Feder, J. (1988). The Cluster Fractal Dimension. In Fractals (pp. 31-40). Springer, Boston, MA.

Firoozabadi, A. (2001). Mechanisms of solution gas drive in heavy oil reservoirs. Journal of Canadian Petroleum Technology, 40(03), 15-20.

Geilikman, M. B., Dusseault, M. B., & Dullien, F. A. (1994, January). Sand production as a viscoplastic granular flow. In *SPE formation damage control symposium*. Society of Petroleum Engineers.

Gondiken, S. (1987, January). Camurlu field immiscible CO2 huff and puff pilot project. In Middle East Oil Show. Society of Petroleum Engineers.

Goodarzi, N. N., & Kantzas, A. (2008). Observations of heavy oil primary production mechanisms from long core depletion experiments. *Journal of Canadian Petroleum Technology*, *47*(04), 46-54.

Goodarzi, N., Bryan, J. L., Mai, A. T., & Kantzas, A. (2005, January). Heavy oil fluid testing with conventional and novel techniques. SPE Paper 97803 presented at the SPE International Thermal Operations and Heavy Oil Symposium, Calgary, Alberta, Canada, November 1-3

Haddad, A. S., & Gates, I. (2015). Modelling of Cold Heavy Oil Production with Sand (CHOPS) using a fluidized sand algorithm. *Fuel*, *158*, 937-947.

Haskin, H. K., & Alston, R. B. (1989). An evaluation of CO2 huff 'n' puff tests in Texas. Journal of petroleum technology, 41(02), 177-184.

Hong, S. Y., Zeng, F., & Du, Z. (2017). Characterization of gas-oil flow in Cyclic Solvent Injection (CSI) for heavy oil recovery. Journal of Petroleum Science and Engineering, 152, 639-652.

Huerta, M., Otero, C., Rico, A., Jimenez, I., de Mirabal, M., & Rojas, G. (1996, January). Understanding foamy oil mechanisms for heavy oil reservoirs during primary production. In *SPE Annual Technical Conference and Exhibition*. Society of Petroleum Engineers.

Istchenko, C. M., & Gates, I. D. (2014). Well/wormhole model of cold heavy-oil production with sand. *SPE Journal*, *19*(02), 260-269.

Istchenko, C. M., & Gates, I. D. (2014). Well/wormhole model of cold heavy-oil production with sand. *Spe Journal*, *19*(02), 260-269.

Istchenko, C., & Gates, I. D. (2012, January). The well-wormhole model of CHOPS: history match and validation. In *SPE Heavy Oil Conference Canada*. Society of Petroleum Engineers.

Ivory, J., Chang, J., Coates, R., & Forshner, K. (2010). Investigation of cyclic solvent injection process for heavy oil recovery. *Journal of Canadian Petroleum Technology*, *49*(09), 22-33.

James, L. A., Rezaei, N., & Chatzis, I. (2007, January). VAPEX, Warm VAPEX, and Hybrid VAPEX-The State of Enhanced Oil Recovery for In Situ Heavy Oils in Canada. In Canadian International Petroleum Conference. Petroleum Society of Canada.

Janet. (2016, Mar 30). Retrieved from http://www.learncheme.com/screencasts/mass-energy-balances.

Jia, X., Gu, Y., & Zeng, F. (2013, September). Pressure pulsing cyclic solvent injection (PP-CSI): A new way to enhance the recovery of heavy oil through solvent-based enhanced oil recovery techniques. In SPE Annual Technical Conference and Exhibition. Society of Petroleum Engineers.

Jia, X., Zeng, F., & Gu, Y. (2015). Gasflooding-assisted cyclic solvent injection (GA-CSI) for enhancing heavy oil recovery. Fuel, 140, 344-353.

Jiang, T., Jia, X., Zeng, F., & Gu, Y. (2013, June). A novel solvent injection technique for enhanced heavy oil recovery: cyclic production with continuous solvent injection. In SPE Heavy Oil Conference-Canada. Society of Petroleum Engineers.

Jian-Yang, Y., Tremblay, B., & Babchin, A. (1999, January). A wormhole network model of cold production in heavy oil. In *International Thermal Operations/Heavy Oil Symposium*. Society of Petroleum Engineers.

Jones, S. F., Evans, G. M., & Galvin, K. P. (1999). Bubble nucleation from gas cavities—a review. *Advances in colloid and interface science*, *80*(1), 27-50.

Kantzas, A., & Brook, G. (2004). Preliminary Laboratory Evaluation of Cold and Post-Cold Production Methods for Heavy Oil Reservoirs Part B: Reservoir Conditions. *Journal of Canadian Petroleum Technology*, *43*(10).

Kariznovi, M., Nourozieh, H., & Abedi, J. (2009). Bitumen characterization and pseudocomponents determination for equation of state modeling. *Energy & Fuels*, *24*(1), 624-633.

Kariznovi, M., Nourozieh, H., & Abedi, J. (2009). Bitumen characterization and pseudocomponents determination for equation of state modeling. *Energy & Fuels*, *24*(1), 624-633.

Kraus, W. P., McCaffrey, W. J., & Boyd, G. W. (1993, January). Pseudo-bubble point model for foamy oils. PETSOC-93-45 presented at the *Annual Technical Meeting*. Petroleum Society of Canada.Calgary, Alberta, Canada, May 9-12.

Kumar, R., Pooladi-Darvish, M., & Okazawa, T. (2002). Effect of depletion rate on gas mobility and solution gas drive in heavy oil. *SPE Journal*, *7*(02), 213-220.

Lebel, J. P. (1994, March). Performance implications of various reservoir access geometries. In *11th Annual Heavy Oil & Oil Sands Tech. Symp., March* (Vol. 2).

Lee, B. I., & Kesler, M. G. (1975). A generalized thermodynamic correlation based on three-parameter corresponding states. *AIChE Journal*, *21*(3), 510-527.

Lillico, D. A., Babchin, A. J., Jossy, W. E., Sawatzky, R. P., & Yuan, J. Y. (2001). Gas bubble nucleation kinetics in a live heavy oil. *Colloids and Surfaces A: Physicochemical and Engineering Aspects*, *192*(1-3), 25-38.

Lim, G. B., Kry, R. P., Harker, B. C., & Jha, K. N. (1995, January). Cyclic stimulation of Cold Lake oil sand with supercritical ethane. In SPE International Heavy Oil Symposium. Society of Petroleum Engineers.

Lin, L., Ma, H., Zeng, F., & Gu, Y. (2014, June). A critical review of the solvent-based heavy oil recovery methods. In SPE Heavy Oil Conference-Canada. Society of Petroleum Engineers.

Liu, P., Wu, Y., & Li, X. (2013). Experimental study on the stability of the foamy oil in developing heavy oil reservoirs. Fuel, 111, 12-19.

Liu, X., & Zhao, G. (2005). A fractal wormhole model for cold heavy oil production. *Journal of Canadian Petroleum Technology*, *44*(09).

Loughead, D. J., & Saltuklaroglu, M. (1992, March). Lloydminster heavy oil production: Why so unusual. In *9th Annual Heavy Oil and Oil Sands Technology Symposium, Calgary* (Vol. 11).

Mai, A., Bryan, J., Goodarzi, N., & Kantzas, A. (2009). Insights into non-thermal recovery of heavy oil. *Journal of Canadian Petroleum Technology*, *48*(03), 27-35.

Maini, B. B. (1999, January). Foamy oil flow in primary production of heavy oil under solution gas drive. In SPE Annual Technical Conference and Exhibition. Society of Petroleum Engineers.

Maini, B. B. (2001). Foamy-oil flow. Journal of Petroleum Technology, 53(10), 54-64.

Maini, B. B., Sarma, H. K., & George, A. E. (1993). Significance of foamy-oil behaviour in primary production of heavy oils. Journal of Canadian petroleum technology, 32(09).

Martinez Gamboa, J.J. and Leung, J.Y. (2019). Design of field-scale cyclic solvent injection processes for post-CHOPS applications. *Canadian Journal of Chemical Engineering* 97: 123-132.

Martinez-Gamboa, J. J., Wang, M., & Leung, J. Y. (2017, May). A Practical Approach for Scale-Up of Solvent Transport Mechanisms in Post-CHOPS EOR Applications. In *SPE Latin America and Caribbean Petroleum Engineering Conference*. Society of Petroleum Engineers.

Mastmann, M., Moustakis, M. L., & Bennion, D. B. (2001). Predicting foamy oil recovery. SPE Paper 68860 presented at the SPE Western Regional Meeting, Bakersfield, California, USA, March 26-30.

Mazurek, K. A. (1994). Sand Removal from a Vertical Heavy Oil Well. *Master of Science thesis in Civil Eng., University of Alberts, Edmonton, Alberts, Canada, Fall*.

McCaffrey, W. J., & Bowman, R. D. (1991, March). Recent successes in primary bitumen production. In *8th Annual Heavy Oil and Oil Sands Technical Symposium, Calgary, Alberta, Canada* (Vol. 14).

Metwally, M., & Solanski, S. C. (1995, January). Heavy Oil Reservoir Mechanisms, Lindbergh and Frog Lake Fields, Alberta Part I: Field Observations and Reservoir Simulation. In *Annual Technical Meeting*. Petroleum Society of Canada.

Oskouei, S. J. P., Zadeh, A. B., & Gates, I. D. (2017). A new kinetic model for non-equilibrium dissolved gas ex-solution from static heavy oil. *Fuel*, *204*, 12-22.

Ostos, A. N. (2004) Effect of capillary number on performance of solution gas drive in heavy oil oil reservoirs.

Ostos, A. N., & Maini, B. B. (2003, January). An integrated experimental study of foamy oil flow during solution gas drive. In Canadian International Petroleum Conference. Petroleum Society of Canada.

Pedersen, K. S., & Fredenslund, A. A. G. E. (1987). An improved corresponding states model for the prediction of oil and gas viscosities and thermal conductivities. *Chemical Engineering Science*, *42*(1), 182-186.

Peng, D. Y., & Robinson, D. B. (1976). A new two-constant equation of state. *Industrial & Engineering Chemistry Fundamentals*, *15*(1), 59-64.

Perkins, T. K., & Johnston, O. C. (1963). A review of diffusion and dispersion in porous media. *Society of Petroleum Engineers Journal*, *3*(01), 70-84.

Plata Sanchez, M. A. (2019). *Experimental Study of Heavy Oil Recovery Mechanisms during Cyclic Solvent Injection Processes* (Master's thesis, Schulich School of Engineering).

Pooladi-Darvish, M., & Firoozabadi, A. (1999). Solution-gas drive in heavy oil reservoirs. Journal of Canadian Petroleum Technology, 38(04).

Qazvini Firouz, A., & Torabi, F. (2012, January). Feasibility study of solvent-based huff-n-puff method (cyclic solvent injection) to enhance heavy oil recovery. In SPE Heavy Oil Conference Canada. Society of Petroleum Engineers.

Rangriz Shokri, A., & Babadagli, T. (2014). Modelling of cold heavy-oil production with sand for subsequent thermal/solvent injection applications. *Journal of Canadian Petroleum Technology*, *53*(02), 95-108.

Rosner, D. E., & Epstein, M. (1972). Effects of interface kinetics, capillarity and solute diffusion on bubble growth rates in highly supersaturated liquids. *Chemical Engineering Science*, *27*(1), 69-88.

Sarma, H., & Maini, B. (1992, January). Role of solution gas in primary production of heavy oils. In SPE Latin America Petroleum Engineering Conference. Society of Petroleum Engineers.

Sawatzky, R. P., Lillico, D. A., London, M. J., Tremblay, B. R., & Coates, R. M. (2002, January). Tracking cold production footprints. In *Canadian International Petroleum Conference*. Petroleum Society of Canada.

Shahvali, M., & Pooladi-Darvish, M. (2009). Dynamic modelling of solution-gas drive in heavy oils. *Journal of Canadian Petroleum Technology*, *48*(12), 39-46.

Shen, C., & Batycky, J. P. (1999). Observation of mobility enhancement of heavy oils flowing through sand pack under solution gas drive. *Journal of Canadian Petroleum Technology*, *38*(04).

Sheng J.J., Maini B.B., Hayes R.E., & Tortike W.S. (1999). A non-equilibrium model to calculate foamy oil properties. *Journal of Canadian Petroleum Technology*, 38(4):38–45.

Sheng, J. J., Maini, B. B., Hayes, R. E., & Tortike, W. S. (1997). Experimental study of foamy oil stability. *Journal of Canadian Petroleum Technology*, *36*(04), 31-37.

Shi, R., & Kantzas, A. (2008, January). Enhanced heavy oil recovery on depleted long core system by CH4 and CO2. In International Thermal Operations and Heavy Oil Symposium. Society of Petroleum Engineers.

Shokri, A. R., & Babadagli, T. (2017). Feasibility assessment of heavy-oil recovery by CO2 injection after cold production with sands: Lab-to-field scale modeling considering non-equilibrium foamy oil behavior. *Applied energy*, *205*, 615-625.

Singhal, A. K., Das, S. K., Leggitt, S. M., Kasraie, M., & Ito, Y. (1996, January). Screening of reservoirs for exploitation by application of steam assisted gravity drainage/vapex processes. In International Conference on Horizontal Well Technology. Society of Petroleum Engineers.

Smith, G. E. (1986). Fluid flow and sand production in heavy oil reservoirs under solution gas drive. SPE 15094. In *56th California Regional Meeting of the Society of Petroleum Engineers, Oakland, California USA*.

Smith, G. E. (1988). Fluid flow and sand production in heavy-oil reservoirs under solution-gas drive. *SPE Production Engineering*, *3*(02), 169-180.

Soh, Y. J., & Babadagli, T. (2017). Cost Effective EOR in Heavy-Oil Containing Sands by Gas Injection: Improvement of the Efficiency of Foamy Flow and Pressurization. SPE Paper 186196 presented at the *SPE/IATMI Asia Pacific Oil & Gas Conference and Exhibition*, Jakrta, Indonesia, October 17-19.

Soh, Y., Rangriz-Shokri, A., & Babadagli, T. (2018). Optimization of methane use in cyclic solvent injection for heavy-oil recovery after primary production through experimental and numerical studies. *Fuel*, *214*, 457-470.

Squires, A. (1993, March). Inter-well tracer results and gel blocking program. In *The 10th Annual Heavy Oil and Oil Sands Technical Symposium, Calgary, Alberta, Canada, Mar* (Vol. 9).

Sun, X., Zhang, Y., Wang, S., Song, Z., Li, P., & Wang, C. (2018). Experimental study and new three-dimensional kinetic modeling of foamy solution-gas drive processes. *Scientific reports*, *8*(1), 4369.

Szekely, J., & Martins, G. P. (1971). Non-equilibrium effects in the growth of spherical gas bubbles due to solute diffusion. *Chemical Engineering Science*, *26*(1), 147-159.

Tang G., Leung T., Castanier L.M., Sahni A., Gadelle F., Kumar M., Kovscek, A.R. (2006). An investigation of the effect of oil composition on heavy oil solution gas drive. *SPE Journal*, 11(1), 58–70.

Tang, G. Q., & Firoozabadi, A. (2005). Effect of GOR, temperature, and initial water saturation on solution-gas drive in heavy-oil reservoirs. Spe Journal, 10(01), 34-43.

Tang, G., & Firoozabadi, A. (2001, January). Effect of GOR, Temperature, and Initial Water Saturation on Solution-Gas Drive in Heavy-Oil Reservoirs. In *SPE Annual Technical Conference and Exhibition*. Society of Petroleum Engineers.

Torabi, F., Jamaloei, B. Y., Stengler, B. M., & Jackson, D. E. (2012). The evaluation of CO 2-based vapour extraction (VAPEX) process for heavy-oil recovery. Journal of Petroleum Exploration and Production Technology, 2(2), 93-105.

Tremblay, B. (2005). Modelling of sand transport through wormholes. *Journal of Canadian Petroleum Technology*, *44*(04).

Tremblay, B. (2007, January). Cold Flow: A Multi-Well Cold Flow (Production) Model. In *Canadian International Petroleum Conference*. Petroleum Society of Canada.

Tremblay, B. S. G. and VU, D., 1999. CT Imaging of Wormhole Growth under Solution Gas Drive. *SPE ResEval&Eng2*, *1*, 37-45.

Tremblay, B., & Oldakowski, K. (2003). Modeling of wormhole growth in cold production. *Transport in porous media*, *53*(2), 197-214.

Tremblay, B., Sedgwick, G., & Forshner, K. (1996). Imaging of sand production in a horizontal sand pack by X-ray computed tomography. SPE formation Evaluation, 11(02), 94-98.

Tremblay, B., Sedgwick, G., & Forshner, K. (1997). Simulation of cold production in heavy-oil reservoirs: Wormhole dynamics. *SPE Reservoir Engineering*, *12*(02), 110-117.

Tremblay, B., Sedgwick, G., & Forshner, K. (1998). Modelling of sand production from wells on primary recovery. *Journal of Canadian Petroleum Technology*, *37*(03).

Twu, C. H., Bluck, D., Cunningham, J. R., & Coon, J. E. (1991). A cubic equation of state with a new alpha function and a new mixing rule. Fluid Phase Equilibria, 69, 33-50.

Uddin, M. (2005, January). Numerical studies of gas exsolution in a live heavy oil reservoir. In *SPE International Thermal Operations and Heavy Oil Symposium*. Society of Petroleum Engineers.

Uddin, M. (2012, January). Modelling of gas exsolution and transport in a live heavy oil reservoir. In *SPE Heavy Oil Conference Canada*. Society of Petroleum Engineers.

Urgelli, D., Durandeau, M., Foucault, H., & Besnier, J. F. (1999, January). Investigation of foamy oil effect from laboratory experiments. In International Thermal Operations/Heavy Oil Symposium. Society of Petroleum Engineers.

Vardoulakis, I., Stavropoulou, M., & Papanastasiou, P. (1996). Hydro-mechanical aspects of the sand production problem. *Transport in porous media*, *22*(2), 225-244.

Wang, H., Zeng, F., & Zhou, X. (2015, June). Study of the non-equilibrium PVT properties of methane-and propane-heavy oil systems. In *SPE Canada Heavy Oil Technical Conference*. Society of Petroleum Engineers.

Wang, Y., & Xue, S. (2002, January). Coupled reservoir-geomechanics model with sand erosion for sand rate and enhanced production prediction. In *International Symposium and Exhibition on Formation Damage Control*. Society of Petroleum Engineers.

Whitson, C. H. (1982). *Effect of physical properties estimation on equation-of-state predictions* (No. CONF-820927-). Rogaland Regional College.

Wikipedia contributors. (2019, June 29). Ideal gas law. In *Wikipedia, The Free Encyclopedia*. Retrieved from https://en.wikipedia.org/w/index.

Witten Jr, T. A., & Sander, L. M. (1981). Diffusion-limited aggregation, a kinetic critical phenomenon. Physical review letters, 47(19), 1400.

Xu, S., & Maini, B. (2007). Investigation of mechanisms involved in generation of foamy oil flow. In Masters Abstracts International (Vol. 45, No. 05).

Yadali Jamaloei, B., Dong, M., Mahinpey, N., & Maini, B. B. (2012). Enhanced cyclic solvent process (ECSP) for heavy oil and bitumen recovery in thin reservoirs. Energy & Fuels, 26(5), 2865-2874.

Yeung, K. C. (1995). Cold flow production of crude bitumen at the Burnt Lake Project, northeastern Alberta (No. CONF-9502114-Vol. 1). UNITAR, New York, NY (United States).

Yu, H. and Leung, J.Y. (2019). A geomechanically-constrained dynamic fractal wormhole growth model for simulating cold heavy oil production with sand simulation. SPE Paper 193893 presented at the SPE Reservoir Simulation Conference, Galveston, Texas, USA, April 10-11.

Yu, Y., Li, L., & Sheng, J. J. (2016, September). Further discuss the roles of soaking time and pressure depletion rate in gas huff-n-puff process in fractured liquid-rich shale reservoirs. In SPE Annual Technical Conference and Exhibition. Society of Petroleum Engineers.

Zhang, M., Du, Z., Zeng, F., Hong, S. Y., & Xu, S. (2016). Upscaling study of the cyclic solvent injection process for post-chops reservoirs through numerical simulation. The Canadian Journal of Chemical Engineering, 94(7), 1402-1412.

Zhou, X., Zeng, F., Zhang, L., & Wang, H. (2016). Foamy oil flow in heavy oil–solvent systems tested by pressure depletion in a sandpack. Fuel, 171, 210-223.